

AlphaToken: Decoupling Adaptation and Stability for Path-Aware Response Token Valuation in LLM Post-Training

Qing Liu, Ou Wu*, Yi Du

Hangzhou Institute for Advanced Study,
University of Chinese Academy of Sciences
liuqing25@mailsucas.ac.cn wuou@ucas.ac.cn

Abstract

Token selection is pivotal for effective LLM post-training. However, existing methods mostly rely on local heuristics and rarely formulate token selection as a principled valuation of individual response tokens. We introduce **AlphaToken**, a response token valuation framework that decouples valuation into **adaptation** (promoting target-task learning) and **stability** (preserving pre-trained capabilities), and makes each objective **path-aware** by combining the direct-path signal from local token gradients with the downstream causal-path signal in autoregressive generation. Since retention data are typically unavailable, AlphaToken approximates stability via a **Fisher-drift proxy** anchored at the pre-trained reference model. For efficient computation, we extend Ghost Dot-Product to token-level valuation. AlphaToken masks low-value response tokens during fine-tuning and preference optimization, concentrating training signals on more valuable positions. Experiments show that AlphaToken improves post-training performance and mitigates catastrophic forgetting. Code at <https://anonymous.4open.science/r/AlphaToken-58A>.

1 Introduction

Large language models (LLMs) are increasingly adapted through post-training to meet evolving domain needs and alignment goals. In practice, supervised fine-tuning (SFT) and preference optimization (PO) have become the dominant adaptation paradigms (Ouyang et al., 2022; Rafailov et al., 2023). Recent work has shown that data utility matters for adaptation, from sample valuation and selection (Liu et al., 2024; Wang et al., 2025a) to emerging token-wise methods that filter tokens for efficiency or robustness (Pang et al., 2025; Simoulin et al., 2024).

Classical formulations build on influence functions and Data Shapley, which estimate each train-

ing sample’s marginal contribution to validation performance (Koh and Liang, 2017; Ghorbani and Zou, 2019). Recent work has improved the scalability of this line for LLM training pipelines. In-Run Data Shapley estimates Shapley-style contributions within a single training trajectory (Wang et al., 2025a), trajectory-aware influence estimation accounts for when a datum appears during optimization (Wang et al., 2025b), and GREATS performs online selection of high-quality batches during LLM training (Wang et al., 2024). While these advances substantially improve scalability, they remain sample-level and cannot capture the heterogeneous contributions that individual response tokens make within a single sequence.

Emerging token selection methods begin to address this issue (Pang et al., 2025; Simoulin et al., 2024). Existing methods typically rely on teacher–student loss gaps, low-perplexity masking, or alignment-specific token weighting (Pang et al., 2025; Wu et al., 2025; Yang et al., 2026a). These criteria are efficient but largely heuristic and single-objective. Although Shapley-style token attribution methods provide a principled view of token importance, they mainly target input-side context attribution and model interpretation (Horovitz and Goldshmidt, 2024; Xiao et al., 2025). This leaves open the need for a principled valuation framework that measures how each response token contributes to LLM post-training.

We propose **AlphaToken**, a fine-grained response token valuation framework for LLM post-training. It decouples the valuation objective into target adaptation and retention stability. AlphaToken achieves path-aware valuation by jointly modeling a response token’s direct-path update signal and its downstream causal-path influence on later predictions in autoregressive generation. Since retention data are typically unavailable in practical post-training, it estimates retention stability with a Fisher-drift proxy anchored at the pre-

*Corresponding author.

trained reference model, enabling stability-aware valuation when no retention examples are available. For efficient computation, we extend Ghost Dot-Product (GDP) to token-level valuation. The composite token values are used to mask low-value response tokens during fine-tuning and preference optimization, concentrating training on positions that better support adaptive and stable post-training. Our key contributions are summarized as follows:

- We formulate response token valuation by decoupling adaptation and retention stability, and make it path-aware by modeling local update and downstream causal signals. We replace inaccessible retention gradients with a Fisher-weighted drift proxy anchored at the pre-trained model.
- Building on GDP for sample-level gradient alignment, we extend it to token-level valuation by supporting causal cross-position alignment through a Value-Propagation approximation and Fisher-drift stability through a new Activation-Parameter contraction.
- Using composite values, we develop a token selection method for post-training scenarios that masks low-utility response tokens in SFT and PO, improving Overall by at least 1.54 points.

2 Related Work

2.1 Data Valuation and Influence Estimation.

Data valuation studies each training example’s contribution to a target metric. Classical approaches center on Data Shapley and scalable variants, including Monte Carlo estimation, acceleration, and semivalue relaxations such as Beta Shapley and Banzhaf values (Ghorbani and Zou, 2019; Jia et al., 2019b; Mitchell et al., 2022; Okhrati and Lipani, 2021; Kwon and Zou, 2022; Wang and Jia, 2023; Li and Yu, 2023). Parallel lines pursue cheaper influence approximations, Bayesian uncertainty formulations, and scalable surrogates such as KNN, distributional, and federated variants (Koh and Liang, 2017; Basu et al., 2021; Nguyen et al., 2023; Jia et al., 2019a; Ghorbani et al., 2020; Wang et al., 2020). Recent work models trajectory dependence through data value embeddings and adaptive reference points for real-time valuation (Wang et al., 2025b; Xu et al., 2025). Although some studies extend Shapley attribution to token-level prompt interpretation, applying such ideas directly to training-time token valuation remains computationally challenging (Horovicz and Goldshmidt, 2024; Xiao

et al., 2025). In-Run Data Shapley mitigates retraining cost by accumulating per-step gradient interactions along a single trajectory (Wang et al., 2025a). In contrast, we estimate objective-aligned token values in one run through gradient alignment with validation utility and a data-free stability proxy.

2.2 Token Selection & Reweighting.

Token-level data selection and reweighting offer an alternative to sample-level filtering for improving post-training efficiency and robustness. Most methods rely on local token heuristics, such as loss- or probability-based scoring, excess-loss and attention-based relevance, regime-aware joint pruning, and perplexity-based masking; similar ideas appear in pretraining and multimodal training (Pang et al., 2025; Liu et al., 2026; Qin et al., 2026; Nagaraj et al., 2025; Wang et al., 2025c; Wu et al., 2025; Lin et al., 2024; Peng et al., 2025). Other lines explore memory-efficient selective backprop, task-structure-aware token weighting, and alignment-oriented token reweighting (Simoulin et al., 2024; Shi et al., 2025; Yang et al., 2026a; Le et al., 2025). In contrast, our method scores tokens using gradient alignment to validation utility and a data-free stability proxy, producing objective-consistent signals for selection.

3 Methodology

3.1 Preliminaries and Problem Formulation

Consider a causal language model parameterized by θ . Let a training instance consist of a prompt $\mathbf{x} = [x_1, \dots, x_P]$ and a response $\mathbf{y} = [y_1, \dots, y_T]$. The training loss $\mathcal{L}_{\text{train}}$ can be either the SFT cross-entropy loss or a preference-optimization loss, with DPO as a representative instantiation. In both instantiations, the loss can be expressed through response-token contributions, allowing us to define a token-level loss ℓ_t for SFT and a token-level pseudo-loss ℓ_t^\pm for DPO. We assign a scalar valuation $\Phi(y_t)$ to each response token to quantify its marginal generalization contribution. Let $\mathcal{D}_{\text{tgt}}^{\text{val}}$ and $\mathcal{D}_{\text{ret}}^{\text{val}}$ denote target-domain and retention validation sets. Balancing target adaptation and retention stability, we define a composite objective

$$J_{\text{val}}(\theta) = J_{\text{tgt}}(\theta; \mathcal{D}_{\text{tgt}}^{\text{val}}) + \lambda \cdot J_{\text{ret}}(\theta; \mathcal{D}_{\text{ret}}^{\text{val}}), \quad (1)$$

where J_{tgt} and J_{ret} denote target and retention validation losses, and λ controls retention strength. Building on the sample-level in-run Shapley view of Wang et al. (2025a), we extend the argument

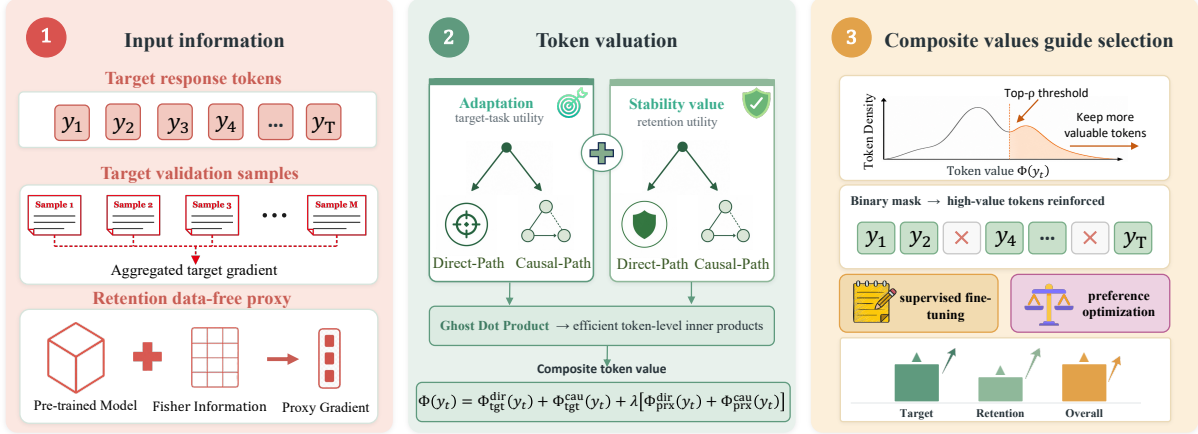


Figure 1: Overview of the AlphaToken framework for selecting high-value response tokens in post-training.

to token-level masking in App. A and define each response token’s value as proportional to the alignment between its training gradient and the composite validation gradient. The valuation thus decomposes into plasticity and stability terms:

$$\Phi(y_t) \propto \langle \nabla_{\theta} \ell_t, \nabla_{\theta} J_{\text{tgt}} \rangle + \lambda \langle \nabla_{\theta} \ell_t, \nabla_{\theta} J_{\text{ret}} \rangle. \quad (2)$$

Directly applying Eq. (2) to token valuation faces three obstacles. **First**, the local gradient $\nabla_{\theta} \ell_t$ undercounts y_t ’s influence, omitting its effect on later predictions through autoregressive context. **Second**, $\nabla_{\theta} J_{\text{ret}}$ depends on the retention validation set $\mathcal{D}_{\text{ret}}^{\text{val}}$, which is typically unavailable in post-training. **Third**, the parameter-space gradient inner products must be computed per response token, prohibitive if token-level gradients are formed.

3.2 Causal Gradient Decomposition

In autoregressive Transformers, a token y_t plays two roles. As a label, it generates the immediate loss ℓ_t at position t . As context, its hidden state influences all future tokens y_k ($k > t$) through self-attention. Routing the loss of each future token backward through the layer- l cross-position transfer from position t to position k and isolating the self-term $k=t$ yields

$$\nabla_{\theta} \ell_t^{\text{tot}} = \nabla_{\theta} \ell_t + \sum_{k=t+1}^T \sum_{l=1}^L \frac{\partial \ell_k}{\partial \mathbf{h}_k^l} \frac{\partial \mathbf{h}_k^l}{\partial \mathbf{h}_t^{l-1}} \frac{\partial \mathbf{h}_t^{l-1}}{\partial \theta}. \quad (3)$$

Eq. (3) isolates the dominant Value-Propagation channel from t to k , derived in App. B.1 by routing each future loss through the cross-position Jacobian and decomposing its attention derivative into the value path. The same chain-rule argument applies to both SFT and DPO losses.

3.3 Data-Free Retention Gradient Proxy

The composite objective in Eq. (2) requires the retention validation gradient $\nabla_{\theta} J_{\text{ret}}$. In realistic post-training, however, the pre-training corpus is unavailable to downstream practitioners due to licensing constraints and closed-source release policies (Kirkpatrick et al., 2017; Sanyal et al., 2025). Thus, we adopt a setting where retention data are unavailable, with access limited to the pre-trained parameters θ_{ref} and the target dataset \mathcal{D}_{tgt} .

Let $\mathcal{L}_{\text{ret}}(\theta)$ denote the unobserved retention loss. Expanding around θ_{ref} :

$$\mathcal{L}_{\text{ret}}(\theta) \approx \mathcal{L}_{\text{ret}}(\theta_{\text{ref}}) + \frac{1}{2}(\theta - \theta_{\text{ref}})^{\top} \mathbf{H}_{\text{ret}}(\theta - \theta_{\text{ref}}), \quad (4)$$

where the first-order term is small to the extent that θ_{ref} approximates a stationary point of \mathcal{L}_{ret} (we bound the residual in App. B.4), and \mathbf{H}_{ret} coincides with the Fisher information at θ_{ref} under the maximum-likelihood calibration condition (Martens, 2020). Replacing \mathbf{H}_{ret} with a model-side Fisher \mathbf{F}_{ref} that requires no retention data yields the data-free retention proxy:

$$J_{\text{prx}}(\theta) = \frac{1}{2}(\theta - \theta_{\text{ref}})^{\top} \mathbf{F}_{\text{ref}}(\theta - \theta_{\text{ref}}). \quad (5)$$

The Fisher information characterizes the likelihood geometry of θ_{ref} , depending on the reference model and prompt distribution rather than retention labels/samples. Here, \mathcal{X} denotes the prompt distribution for Monte-Carlo Fisher construction, instantiated by prompts from \mathcal{D}_{tgt} . To avoid the bias of the empirical Fisher far from a local optimum (Kunstner et al., 2019), we adopt the Monte-Carlo Fisher with labels self-sampled from $p_{\theta_{\text{ref}}}$:

$$\mathbf{F}_{\text{ref}} = \text{Diag} \left(\mathbb{E}_{\mathbf{x} \sim \mathcal{X}, \tilde{\mathbf{y}} \sim p_{\theta_{\text{ref}}}(\cdot|\mathbf{x})} \left[\nabla_{\theta} \log p_{\theta_{\text{ref}}}(\tilde{\mathbf{y}}|\mathbf{x})^{\odot 2} \right] \right),$$

\mathbf{F}_{ref} is computed once before training and cached.

Differentiating Eq. (5) gives

$$\mathbf{g}_{\text{prx}} \triangleq \nabla_{\boldsymbol{\theta}} J_{\text{prx}}(\boldsymbol{\theta}) = \mathbf{F}_{\text{ref}}(\boldsymbol{\theta} - \boldsymbol{\theta}_{\text{ref}}), \quad (6)$$

which acts as a virtual retention validation gradient: substituting \mathbf{g}_{prx} for $\nabla_{\boldsymbol{\theta}} J_{\text{ret}}$ in Eq. (2) preserves the alignment formulation while removing retention data dependency. Tokens whose training gradients align with \mathbf{g}_{prx} contract the Fisher-weighted drift from $\boldsymbol{\theta}_{\text{ref}}$ and are therefore retention-friendly. The corresponding retention valuation reads

$$\Phi_{\text{prx}}(y_t) \triangleq \langle \nabla_{\boldsymbol{\theta}} \ell_t^{\text{tot}}, \mathbf{g}_{\text{prx}} \rangle. \quad (7)$$

By the linearity of the inner product and the direct/causal split of $\nabla_{\boldsymbol{\theta}} \ell_t^{\text{tot}}$ in Eq. (3), $\Phi_{\text{prx}}(y_t) = \Phi_{\text{prx}}^{\text{dir}}(y_t) + \Phi_{\text{prx}}^{\text{cau}}(y_t)$.

3.4 Ghost Dot-Product Approximation

Realizing Eq. (2) requires token-level inner products for direct target alignment, causal future-token alignment, and retention alignment with \mathbf{g}_{prx} . Naively materializing per-token parameter gradients costs $\mathcal{O}(T|\boldsymbol{\theta}|)$, which is prohibitive at LLM scale. We compute all three with a unified GDP family: the direct activation–activation (A–A) form adapts the example-level construction of Wang et al. (2025a) to tokens, while the causal A–A form and the activation–parameter (A–P) proxy form are new. Scores are aggregated over the last K layers \mathcal{S} .

Direct token alignment (A–A). For a linear layer \mathbf{W}^l , the token-level loss yields a rank-1 weight gradient $\nabla_{\mathbf{W}^l} \ell_t = \boldsymbol{\delta}_t^l \otimes \mathbf{h}_t^l$ with input activation \mathbf{h}_t^l and output error $\boldsymbol{\delta}_t^l \triangleq \partial \ell_t / \partial \mathbf{h}_t^l$. Following Wang et al. (2025a), the Frobenius inner product factorizes into two activation-space dot products. Concatenating a small fixed validation batch with the training batch in a single backward pass (Wang et al., 2024) yields per-token training signals $(\boldsymbol{\delta}_t^l, \mathbf{h}_t^l)$ and per-validation-token target signals $(\boldsymbol{\delta}_v^l, \mathbf{h}_v^l)_{v \in \mathcal{V}_{\text{tgt}}}$ from the same cache, where \mathcal{V}_{tgt} denotes the held-out target validation token set. Summing over layers and averaging over \mathcal{V}_{tgt} , the direct target valuation reads

$$\Phi_{\text{tgt}}^{\text{dir}}(y_t) = \frac{1}{|\mathcal{V}_{\text{tgt}}|} \sum_{v \in \mathcal{V}_{\text{tgt}}} \sum_{l \in \mathcal{S}} \langle \boldsymbol{\delta}_t^l, \boldsymbol{\delta}_v^l \rangle \langle \mathbf{h}_t^l, \mathbf{h}_v^l \rangle. \quad (8)$$

Causal token alignment (A–A causal). The cross-position Jacobian is dense; we approximate it by retaining only linear Value-Propagation through \mathbf{W}_V^l and omitting nonlinear Score-Propagation, whose magnitude decays as $\mathcal{O}(1/\sqrt{d_h})$ under saturated attention, where d_h is the attention-head

dimension (App. B.3). This yields $\nabla_{\mathbf{W}_V^l} \ell_{t \rightarrow k} \approx \alpha_{t \rightarrow k}^l (\boldsymbol{\delta}_k^l \otimes \mathbf{h}_t^{l-1})$ with attention weight $\alpha_{t \rightarrow k}^l$. The activation-space factorization, averaged over \mathcal{V}_{tgt} , gives the causal target valuation

$$\Phi_{\text{tgt}}^{\text{cau}}(y_t) = \frac{1}{|\mathcal{V}_{\text{tgt}}|} \sum_{v \in \mathcal{V}_{\text{tgt}}} \sum_{l \in \mathcal{S}, k} \alpha_{t \rightarrow k}^l \langle \boldsymbol{\delta}_k^l, \boldsymbol{\delta}_v^l \rangle \langle \mathbf{h}_t^{l-1}, \mathbf{h}_v^{l-1} \rangle, \quad (9)$$

with $k \in (t, \min(t+W, T)]$ for causal window W .

Retention proxy (A–P). The retention gradient \mathbf{g}_{prx} is a fixed parameter-space vector and is not the back-propagation output of any sample-level loss; it admits no activation-only factorization. We instead contract the rank-1 token gradient against \mathbf{g}_{prx} directly. For each linear layer, define

$$\mathbf{V}^l \triangleq \mathbf{F}_{\mathbf{W}^l} \odot (\mathbf{W}^l - \mathbf{W}_{\text{ref}}^l), \quad (10)$$

the layer- l slice of \mathbf{g}_{prx} , where $\mathbf{F}_{\mathbf{W}^l} \triangleq \text{Diag}(\mathbf{F}_{\text{ref}})|_{\mathbf{W}^l}$ and refresh once per training step. Exploiting the rank-1 form of $\nabla_{\mathbf{W}^l} \ell_t$,

$$\langle \nabla_{\mathbf{W}^l} \ell_t, \mathbf{V}^l \rangle_F = (\boldsymbol{\delta}_t^l)^\top \mathbf{V}^l \mathbf{h}_t^l, \quad (11)$$

which evaluates as a single matrix–vector product per layer per token without ever forming a model-sized intermediate. Stacking the activations of T tokens into $\mathbf{H}^l \in \mathbb{R}^{T \times d_{\text{in}}}$ and the errors into $\boldsymbol{\Delta}^l \in \mathbb{R}^{T \times d_{\text{out}}}$, all T scores collapse to one GEMM $\mathbf{H}^l (\mathbf{V}^l)^\top \in \mathbb{R}^{T \times d_{\text{out}}}$ followed by an element-wise product with $\boldsymbol{\Delta}^l$, costing $\mathcal{O}(T d_{\text{in}} d_{\text{out}})$ —identical in order to the activation–activation case and far below the $\mathcal{O}(T|\boldsymbol{\theta}|)$ baseline. The direct proxy term follows Eq. (11), while replacing $\boldsymbol{\delta}_t^l$ and \mathbf{h}_t^l with $\alpha_{t \rightarrow k}^l \boldsymbol{\delta}_k^l$ and \mathbf{h}_t^{l-1} gives $\Phi_{\text{prx}}^{\text{cau}}(y_t)$ analogously to Eq. (9) (see App. B.2).

Total token valuation. Substituting the path-aware gradient $\nabla_{\boldsymbol{\theta}} \ell_t^{\text{tot}}$ and the retention proxy \mathbf{g}_{prx} into the valuation template Eq. (2), we obtain the AlphaToken valuation:

$$\Phi(y_t) = \Phi_{\text{tgt}}^{\text{dir}}(y_t) + \Phi_{\text{tgt}}^{\text{cau}}(y_t) + \lambda [\Phi_{\text{prx}}^{\text{dir}}(y_t) + \Phi_{\text{prx}}^{\text{cau}}(y_t)]. \quad (12)$$

By Eq. (7), the retention bracket is $\langle \nabla_{\boldsymbol{\theta}} \ell_t^{\text{tot}}, \mathbf{g}_{\text{prx}} \rangle$. All four scores reuse one cached forward/backward pass; the extra cost is evaluating the fixed validation batch in the joint forward/backward pass to obtain $(\boldsymbol{\delta}_v^l, \mathbf{h}_v^l)_{v \in \mathcal{V}_{\text{tgt}}}$, plus one GEMM per linear layer for A–P contraction with \mathbf{V}^l .

3.5 Value-Aware Post-Training

Given the per-token value $\Phi(y_t)$, AlphaToken allocates gradient flow to the most informative response tokens via binary masking.

Algorithm 1 Value-Aware Post-Tuning

Require: Dataset $\mathcal{D}_{\text{tgt}}^{\text{train}}$, pre-trained θ_{ref} , Fisher F_{ref} , validation set $\mathcal{D}_{\text{tgt}}^{\text{val}}$, ratio ρ , layer set \mathcal{S} , learning rate η , weight λ , window W .

Ensure: Optimized parameters θ^* .

- 1: **for** each training step **do**
 - 2: Sample minibatch $\mathcal{B} \sim \mathcal{D}_{\text{tgt}}^{\text{train}}$.
 - 3: Compute $\Phi_{\text{tgt}}^{\text{dir/cau}}$ by Eqs. (8), (9).
 - 4: Refresh $\mathbf{V}^l = \mathbf{F}_{\mathbf{W}^l} \odot (\mathbf{W}^l - \mathbf{W}_{\text{ref}}^l)$.
 - 5: Compute $\Phi_{\text{prx}}^{\text{dir/cau}}$ via Eq. (11).
 - 6: Aggregate $\Phi(y_t)$ via Eq. (12); mask $m_t = \mathbb{I}[\Phi(y_t) \geq \tau_\rho]$ at within-batch top- ρ .
 - 7: Form $\mathcal{L} = \mathcal{L}_{\text{Alpha-SFT}}$ by Eq. (13) or $\mathcal{L}_{\text{Alpha-DPO}}$ by Eq. (14).
 - 8: $\theta \leftarrow \theta - \eta \nabla_{\theta} \mathcal{L}$.
 - 9: **end for**
 - 10: **return** θ^* .
-

Supervised Fine-tuning (SFT). With a within-batch top- ρ threshold τ_ρ , the value-aware loss is

$$\mathcal{L}_{\text{Alpha-SFT}}(\theta) = \sum_{t=1}^T \mathbb{I}[\Phi(y_t) \geq \tau_\rho] \ell_t(\theta), \quad (13)$$

with $\ell_t(\theta) = -\log \pi_{\theta}(y_t | \mathbf{x}, \mathbf{y}_{<t})$. Low-utility tokens are skipped; gradient compute is reallocated to high-value positions.

Direct preference optimization (DPO). Extending the mask to DPO requires unrolling the sequence-level loss to per-token contributions. Given triplet $(\mathbf{x}, \mathbf{y}^+, \mathbf{y}^-)$, with s and $\omega \triangleq \beta \sigma(-s)$ as in standard DPO (Rafailov et al., 2023),

$$\nabla_{\theta} \ell^{\text{DPO}} = \omega (\nabla_{\theta} [-\log \pi_{\theta}(\mathbf{y}^+ | \mathbf{x})] - \nabla_{\theta} [-\log \pi_{\theta}(\mathbf{y}^- | \mathbf{x})]),$$

so the layer-wise error signal scales linearly as $\delta_t^{(l)\pm} = \pm \omega \tilde{\delta}_t^{(l)\pm}$, where $\tilde{\delta}_t^l$ is the standard SFT-style error signal. We then compute $\Phi(y_t^{\pm})$ via Eq. (12) using the scaled $\delta_t^{(l)\pm}$, and gate gradient flow with detached masks $m_t^{\pm} = \text{sg}(\mathbb{I}[\Phi(y_t^{\pm}) \geq \tau_\rho^{\pm}])$ and detached weight $\omega_{\text{sg}} = \text{sg}(\omega)$, where $\text{sg}(\cdot)$ denotes the stop-gradient operator:

$$\mathcal{L}_{\text{Alpha-DPO}}(\theta) = \mathbb{E} \left[\omega_{\text{sg}} \sum_t (m_t^+ \ell_t^+(\theta) - m_t^- \ell_t^-(\theta)) \right], \quad (14)$$

with $\ell_t^{\pm}(\theta) = -\log \pi_{\theta}(y_t^{\pm} | \mathbf{x}, \mathbf{y}_{<t}^{\pm})$. The sequence-level DPO coefficient is computed from the unmasked preference logit and detached, so masking applies only to the per-token surrogate update. High-value tokens in \mathbf{y}^+ are reinforced, while selected tokens in \mathbf{y}^- provide focused negative

evidence whose likelihood is reduced, mitigating alignment tax without an explicit regularizer. Algorithm 1 summarizes the unified procedure.

4 Theoretical Analysis

We justify the two approximations underlying AlphaToken: the Value-Propagation simplification of cross-position Jacobians and the data-free Fisher-drift proxy for retention stability. Complete bounds and proofs are in Appendix B.

Value-Propagation approximation. The exact causal gradient requires back-propagating through the full softmax attention score matrix. Retaining only the dominant linear value-projection path incurs a controlled $\mathcal{O}(1/\sqrt{d_h})$ operator-norm error, $\|\mathbf{J}_{k,t}^l - \hat{\mathbf{J}}_{k,t}^l\|_{\text{op}} \leq (C/\sqrt{d_h}) \alpha_{t \rightarrow k}^l \|\mathbf{v}_t - \mathbf{o}_k\|$, that vanishes under both sparse and saturated attention: small attention weights suppress the prefactor, while saturated attention forces the output to collapse to the value vector. See Appendix B.3.

Data-free retention bound. The Fisher-drift proxy approximates the true retention gradient without any retention data. Their discrepancy is bounded by three terms, $\|\mathbf{r}_0\| + \|\mathbf{H}_{\text{ret}} - \mathbf{F}_{\text{ref}}\| \|\Delta\theta\| + \frac{M_3}{2} \|\Delta\theta\|^2$: **(I)** a first-order residual at the reference checkpoint; **(II)** a Fisher-Hessian mismatch decomposing into a calibration gap (Martens, 2020) and a Wasserstein distance (Kunstner et al., 2019), both controllable without retention data; and **(III)** a third-order remainder suppressed by value-aware masking because it limits parameter drift. None requires expectations over the unobserved retention dataset \mathcal{D}_{ret} . See Appendix B.4.

5 Experiments

We design a series of experiments to answer the following four questions: **1** Does AlphaToken improve the trade-off between target adaptation and stability under both SFT and preference optimization? **2** Do the estimated token values provide an informative ranking for token selection? **3** How much does each factorized component contribute, including adaptation vs. stability and direct vs. causal paths? **4** How sensitive is AlphaToken to its key design choices, and what computational overhead does it introduce?

Table 1: Fine-Tuning main results. Pre-trained models are excluded from color ranking. The best and second-best results are highlighted in red and blue, respectively.

Model	Method	General Capability Acc. (%)					Target (%)	Overall
		ARC-C	HellaSwag	MMLU	GSM8K	Avg.	HE	Avg.
Llama-3.2-3B	Pre-trained	43.00±0.00	55.82±0.00	56.54±0.00	27.45±0.00	45.70±0.00	28.66±0.00	37.18±0.00
	Standard FT	39.97±0.47	52.45±0.34	48.23±0.43	20.58±0.34	40.31±0.20	44.60±0.48	42.46±0.26
	LoRA ICLR 2022	41.62±0.39	53.32±0.34	50.42±0.35	21.00±0.39	41.59±0.18	41.46±0.40	41.53±0.22
	LESS ICML 2024	42.62±0.34	54.62±0.30	53.57±0.31	22.61±0.23	43.36±0.15	42.24±0.34	42.80±0.19
	Token Cleaning ICML 2025	41.77±0.37	52.20±0.21	53.94±0.33	26.00±0.24	43.48±0.15	40.93±0.36	42.21±0.19
	STM NeurIPS 2025	42.02±0.35	54.61±0.34	55.30±0.30	26.22±0.34	44.54±0.17	41.54±0.35	43.04±0.19
	XTF ICLR 2026	40.47±0.41	52.03±0.29	50.69±0.36	22.58±0.29	41.44±0.17	42.02±0.39	41.73±0.21
	ssTOKEN ICLR 2026	41.94±0.37	53.37±0.31	53.10±0.33	25.38±0.32	43.45±0.17	42.93±0.38	43.19±0.20
	AlphaToken	42.76±0.31	55.48±0.26	56.22±0.28	27.40±0.31	45.47±0.15	43.98±0.40	44.73±0.21
	Gemma-3-4B	Pre-trained	51.45±0.00	56.86±0.00	59.60±0.00	37.00±0.00	51.23±0.00	35.36±0.00
Standard FT		50.17±0.45	52.63±0.38	53.87±0.40	24.12±0.28	45.20±0.19	58.79±0.49	52.00±0.26
LoRA ICLR 2022		49.19±0.36	55.81±0.28	56.71±0.32	31.44±0.42	48.29±0.17	54.62±0.51	51.46±0.27
LESS ICML 2024		50.77±0.34	56.45±0.30	54.26±0.29	31.98±0.37	48.37±0.16	57.17±0.44	52.77±0.23
Token Cleaning ICML 2025		50.85±0.38	55.84±0.23	55.94±0.34	33.00±0.38	48.91±0.17	57.12±0.44	53.02±0.23
STM NeurIPS 2025		50.30±0.40	56.19±0.34	57.30±0.27	36.21±0.38	50.00±0.18	54.01±0.51	52.01±0.27
XTF ICLR 2026		48.70±0.39	53.88±0.35	56.33±0.33	34.44±0.39	48.34±0.18	56.64±0.52	52.49±0.28
ssTOKEN ICLR 2026		50.58±0.37	54.31±0.31	57.34±0.34	35.20±0.40	49.36±0.18	57.45±0.51	53.41±0.27
AlphaToken		51.10±0.30	55.12±0.29	58.22±0.28	36.58±0.46	50.26±0.17	62.15±0.34	56.21±0.19
Qwen-3.5-9B		Pre-trained	54.27±0.00	59.67±0.00	72.62±0.00	86.20±0.00	68.19±0.00	60.96±0.00
	Standard FT	49.25±0.41	54.21±0.33	66.24±0.36	77.92±0.31	61.91±0.18	75.94±0.41	68.93±0.22
	LoRA ICLR 2022	51.27±0.33	56.40±0.32	69.60±0.29	81.97±0.24	64.81±0.15	70.20±0.24	67.51±0.14
	LESS ICML 2024	50.24±0.30	57.11±0.31	69.68±0.26	81.23±0.37	64.57±0.16	72.82±0.35	68.70±0.19
	Token Cleaning ICML 2025	52.76±0.35	55.02±0.34	68.91±0.31	83.54±0.44	65.06±0.18	73.58±0.32	69.32±0.18
	STM NeurIPS 2025	52.65±0.28	57.43±0.32	70.63±0.25	82.87±0.41	65.90±0.16	71.93±0.46	68.92±0.24
	XTF ICLR 2026	52.56±0.36	57.61±0.34	70.51±0.30	83.59±0.43	66.07±0.18	73.61±0.41	69.84±0.22
	ssTOKEN ICLR 2026	51.39±0.37	55.17±0.35	70.52±0.31	82.72±0.42	64.95±0.18	75.21±0.41	70.08±0.22
	AlphaToken	53.13±0.27	57.71±0.31	71.20±0.25	83.14±0.39	66.30±0.15	78.88±0.34	72.59±0.19

5.1 Setup

Models and training pipelines. We evaluate three representative pre-trained backbones of different scales: Llama-3.2-3B (Grattafiori et al., 2024), Gemma-3-4B (Team et al., 2025), and Qwen-3.5-9B (Qwen Team, 2026). For SFT, each model is directly fine-tuned on the target corpus. For preference optimization, we first perform a uniform SFT warm-up on UltraChat-200k (Ding et al., 2023) to obtain a chat-capable reference model, and then optimize on UltraFeedback (Bartolome et al., 2023). Implementation details are provided in App. C.4.

Datasets & Evaluation Metrics. For SFT, we use Magicoder (Wei et al., 2024) as the target corpus and evaluate target-task adaptation on HumanEval (Chen et al., 2021). For preference optimization, we train on UltraFeedback and evaluate preference learning on AlpacaEval 2 (Li et al., 2023) and Arena-Hard v0.1 (Li et al., 2024). Retention is measured by general-capability accuracy on ARC-C (Clark et al., 2018), HellaSwag (Zellers et al., 2019), MMLU (Hendrycks et al., 2021), and GSM8K (Cobbe et al., 2021). Overall denotes the average of the target-side and retention-side scores (Sanyal et al., 2025).

Baselines & Implementation Details. For SFT, we compare against Standard FT, LoRA (Hu et al., 2022), LESS (Xia et al., 2024), Token Cleaning (Pang et al., 2025), STM (Wu et al.,

2025), XTF (Yang et al., 2026b), and ssTOKEN (Qin et al., 2026). For PO, we compare against DPO (Rafailov et al., 2023), SePO (Yang et al., 2025), TI-DPO (Yang et al., 2026a), and ConfPO (Yoon et al., 2025). All baselines are implemented under the matched backbone, data split, training budget, tokenizer, optimizer, scheduler, and evaluation protocol. For AlphaToken, we by default set the selection ratio $\rho=0.5$, the stability weight $\lambda=1.5$, the causal window $W=32$, and use the last $K=3$ Transformer layers for GDP across all backbones. All results are averaged over three seeds, with stds reported where shown. Full hyperparameters and baseline reproduction details are reported in App. C. All experiments are conducted on $4\times$ NVIDIA A100 GPUs.

Validation and Monte-Carlo Fisher construction. For each target training set \mathcal{D}_{tgt} , we randomly hold out a 32-sample target-validation subset $\mathcal{D}_{\text{tgt}}^{\text{val}}$ prior to training. In addition, 1,000 prompts are sampled from \mathcal{D}_{tgt} to construct the diagonal Monte-Carlo Fisher \mathbf{F}_{ref} ; these prompts are excluded from training to avoid any parameter updates. The training pool is therefore

$$\mathcal{D}_{\text{tgt}}^{\text{train}} = \mathcal{D}_{\text{tgt}} \setminus (\mathcal{D}_{\text{tgt}}^{\text{val}} \cup \mathcal{D}_{\text{ref}}^{\text{Fisher}}),$$

where $\mathcal{D}_{\text{ref}}^{\text{Fisher}}$ denotes the 1,000 prompts randomly sampled for Fisher matrix construction. The target-validation samples are used only to compute target-

Table 2: Preference Optimization main results. Base denotes the UltraChat-200k warm-started reference before preference optimization. The best and second-best results are highlighted in red and blue, respectively.

Method	General Capability Acc. (%)					Preference Win Rate (%)			Overall
	ARC-C	HellaSwag	MMLU	GSM8K	Avg.	AE2	A-Hard	Avg.	Avg.
Llama-3.2-3B									
Base	41.19 \pm 0.00	53.76 \pm 0.00	48.99 \pm 0.00	23.68 \pm 0.00	41.91 \pm 0.00	4.10 \pm 0.00	2.10 \pm 0.00	3.10 \pm 0.00	22.51 \pm 0.00
DPO NeurIPS 2023	39.84 \pm 0.52	52.20 \pm 0.50	47.62 \pm 0.38	21.05 \pm 0.68	40.18 \pm 0.49	12.86 \pm 0.38	9.40 \pm 0.47	11.13 \pm 0.30	25.66 \pm 0.29
ConfPO ICML 2025	40.68\pm0.63	51.02 \pm 0.49	47.48 \pm 0.38	22.65\pm0.74	40.46 \pm 0.50	16.83 \pm 0.49	13.30 \pm 0.36	15.07 \pm 0.30	27.77\pm0.29
SePO EMNLP 2025	37.15 \pm 0.50	50.48 \pm 0.48	46.01 \pm 0.40	20.72 \pm 0.70	38.59 \pm 0.50	17.95\pm0.44	13.90\pm0.41	15.93\pm0.30	27.26 \pm 0.29
TI-DPO ICLR 2026	40.42 \pm 0.55	52.77\pm0.51	48.25\pm0.39	22.26 \pm 0.72	40.93\pm0.50	15.59 \pm 0.33	12.20 \pm 0.48	13.90 \pm 0.29	27.42 \pm 0.29
AlphaToken	40.95\pm0.63	53.36\pm0.47	48.03\pm0.39	23.15\pm0.71	41.37\pm0.49	19.44\pm0.47	15.80\pm0.39	17.62\pm0.31	29.50\pm0.29
Gemma-3-4B									
Base	50.66 \pm 0.00	51.60 \pm 0.00	52.86 \pm 0.00	25.42 \pm 0.00	45.14 \pm 0.00	10.87 \pm 0.00	6.30 \pm 0.00	8.59 \pm 0.00	26.87 \pm 0.00
DPO NeurIPS 2023	49.42 \pm 0.51	50.58 \pm 0.50	51.35 \pm 0.40	22.86 \pm 0.77	43.55 \pm 0.51	22.48 \pm 0.41	19.40 \pm 0.35	20.94 \pm 0.27	32.25 \pm 0.29
ConfPO ICML 2025	50.20\pm0.61	51.28\pm0.51	52.34\pm0.40	23.38 \pm 0.82	44.30\pm0.51	28.45\pm0.48	24.90 \pm 0.37	26.68\pm0.30	35.49\pm0.30
SePO EMNLP 2025	47.78 \pm 0.53	48.82 \pm 0.48	50.72 \pm 0.41	23.45 \pm 0.79	42.69 \pm 0.51	27.83 \pm 0.34	25.40\pm0.49	26.62 \pm 0.30	34.66 \pm 0.30
TI-DPO ICLR 2026	50.02 \pm 0.49	51.05 \pm 0.49	52.10\pm0.39	23.96\pm0.80	44.28 \pm 0.51	26.77 \pm 0.45	23.20 \pm 0.31	24.99 \pm 0.27	34.64 \pm 0.29
AlphaToken	50.48\pm0.61	51.46\pm0.47	51.68 \pm 0.39	24.06\pm0.81	44.42\pm0.51	31.86\pm0.49	27.40\pm0.41	29.63\pm0.32	37.03\pm0.30
Qwen-3.5-9B									
Base	50.41 \pm 0.00	54.18 \pm 0.00	67.27 \pm 0.00	78.18 \pm 0.00	62.51 \pm 0.00	15.84 \pm 0.00	12.40 \pm 0.00	14.12 \pm 0.00	38.32 \pm 0.00
DPO NeurIPS 2023	49.02 \pm 0.52	52.84 \pm 0.49	65.71 \pm 0.36	75.62 \pm 0.89	60.80 \pm 0.45	34.41 \pm 0.42	29.80 \pm 0.36	32.11 \pm 0.28	46.46 \pm 0.27
ConfPO ICML 2025	49.85\pm0.56	53.72\pm0.49	66.02 \pm 0.34	76.36 \pm 0.93	61.49 \pm 0.46	35.84 \pm 0.47	31.80\pm0.40	33.82 \pm 0.31	47.66\pm0.28
SePO EMNLP 2025	48.34 \pm 0.50	52.15 \pm 0.50	65.05 \pm 0.35	75.31 \pm 0.91	60.21 \pm 0.45	36.46\pm0.39	31.60 \pm 0.48	34.03\pm0.31	47.12 \pm 0.27
TI-DPO ICLR 2026	49.62 \pm 0.62	53.48 \pm 0.48	66.38\pm0.36	76.94\pm0.92	61.61\pm0.45	34.16 \pm 0.33	30.50 \pm 0.45	32.33 \pm 0.28	46.97 \pm 0.26
AlphaToken	50.18\pm0.54	54.02\pm0.48	67.05\pm0.35	77.92\pm0.90	62.29\pm0.45	38.76\pm0.49	34.60\pm0.37	36.68\pm0.31	49.49\pm0.27

side gradients for token valuation and do not directly contribute to the masked training loss.

5.2 Main Results

Supervised fine-tuning. Table 1 reports SFT results. AlphaToken achieves the best Overall across three backbones, improving over the strongest baseline by 1.54, 2.80, and 2.51 points on Llama-3.2-3B, Gemma-3-4B, and Qwen-3.5-9B, respectively. These gains do not come at the cost of target adaptation: AlphaToken ranks first on HumanEval for Gemma-3-4B and Qwen-3.5-9B and second on Llama-3.2-3B, while matching or exceeding the strongest competitor on General Capability Avg. Baselines such as Token Cleaning and STM rely on a local heuristic that entangles adaptation and retention. AlphaToken derives a principled valuation $\Phi(y_t)$ via gradient alignment with the validation objective, scoring adaptation and retention separately, allowing masking to improve both. See App. D.7 for MetaMathQA results.

Preference optimization. Table 2 reports the DPO comparison after UltraChat-200k warm-up. AlphaToken attains the best Overall score on all three backbones, improving over the strongest competing baseline by 1.73, 1.54, and 1.83 points. The improvement is two-sided: Preference Avg. rises by 2.55, 2.95, and 2.86 points, while General Capability Avg. rises by 0.91, 0.12, and 0.80 points. This contrasts with the standard DPO row, where preference-side gains incur visible retention regression, and with ConfPO, SePO, and TI-DPO, which mitigate the alignment tax only on one side. AlphaToken instead masks both branches by the com-

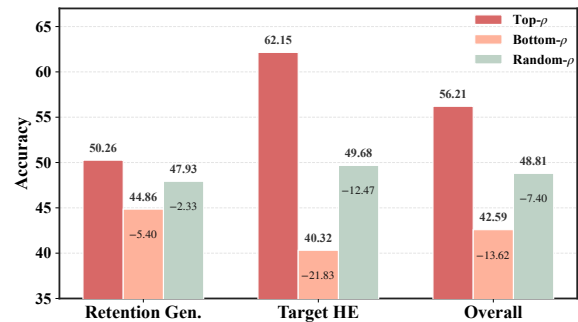


Figure 2: Token-policy intervention on Gemma-3-4B/SFT. All policies use the same $\rho=0.5$.

posite valuation $\Phi(y_t)$, yielding the two-sided gain observed above.

5.3 Token Ranking Effectiveness

We test whether the value score Φ induces a meaningful token ranking. On Gemma-3-4B/SFT, we compare the default Top- ρ policy with two controls under the same retained-token ratio: Random- ρ , which selects tokens at random, and Bottom- ρ , which selects the lowest-scored tokens. As shown in Fig. 2, Top- ρ substantially outperforms both controls. It improves the Overall score by 13.62 points over Bottom- ρ and by 7.40 points over Random- ρ , with consistent gains in retention and target accuracy. This clearly verifies that AlphaToken’s score is not merely a masking heuristic: high-scored tokens are indeed more beneficial for training than low-scored or randomly selected tokens.

5.4 Component Ablations

Table 3 ablates AlphaToken on Gemma-3-4B/SFT along two axes: the objective axis (adaptation vs.

Table 3: Component ablations on Gemma-3-4B/SFT. AlphaToken decomposes token value along two axes: the objective axis, i.e., adaptation vs. stability, and the path axis, i.e., direct vs. causal.

Ablation Axis	Variant	Gen.	Target HE	Overall
Full design	Full AlphaToken	50.26	62.15	56.21
Objective	Adaptation-only	46.64	65.48	56.06
	Stability-only	52.18	58.72	55.45
Path	Direct-only	50.38	59.06	54.72
	Causal-only	49.54	56.34	52.94

stability) specifies what a token’s value rewards, and the path axis (direct vs. causal) specifies how that value is attributed along the trajectory. The full design attains 56.21 Overall, above every single-axis variant. On the objective axis, Adaptation-only gains +3.33 on Target HE but loses -3.62 on Gen., while Stability-only shows the mirror pattern ($+1.92/-3.43$). The oppositely signed shifts indicate that the two terms encode opposing update directions, toward the target vs. preserving the pretraining distribution, so only their combination yields a balanced point. On the path axis, Direct-only lowers Overall by 1.49 with the loss concentrated on Target HE, whereas Causal-only degrades it by 3.27, hurting both, indicating the direct signal is a low-variance backbone and the causal signal supplies long-range credit assignment, and only their combination recovers 56.21.

5.5 Sensitivity and Computational Cost

Figure 3 studies AlphaToken’s key hyperparameters ($\rho, \lambda, W, K, B_{\text{val}}$) and per-step cost on Llama-3.2-3B/SFT. For the selection ratio ρ , retention decreases and adaptation increases monotonically as ρ grows, and overall score peaks at $\rho=0.5$. The stability weight λ trades retention against adaptation, with overall score peaking at $\lambda=1.5$. For the causal window, indicators plateau around $W=32$; further enlargement still improves accuracy marginally but incurs additional compute. For the scoring depth, $K=3$ marks a clear knee beyond which gains diminish while step time keeps growing roughly linearly in K . For the target-validation batch, performance gains saturate at $B_{\text{val}}=32$.

5.6 Component-wise Token Attribution

We visualize the four AlphaToken scoring components on a representative dynamic-programming explanation from the *Last Stone Weight II* task. Scores are normalized within the same response

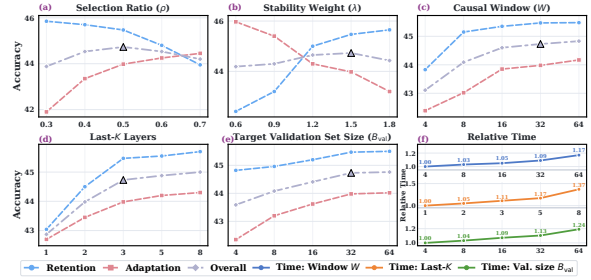


Figure 3: Parameter sensitivity of AlphaToken on Llama-3.2-3B/SFT and relative time along W, K, B_{val} .

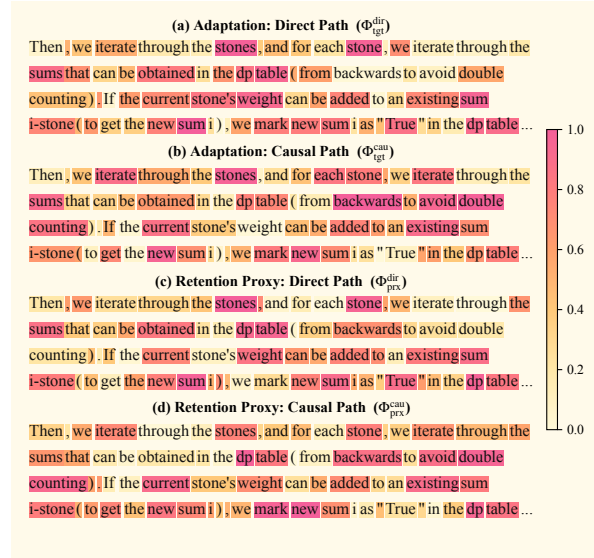


Figure 4: Component-wise token attribution on a dynamic-programming explanation. The same response segment is visualized under four components.

segment, with darker colors indicating higher relative importance. Figure 4 shows that the components capture distinct token-level signals. The adaptation direct path highlights task-relevant tokens such as *stones*, *sums*, *dp table*, and *weight*, while the adaptation causal path emphasizes reasoning-organizing tokens such as *iterate*, *backwards*, and *avoid double counting*. The retention-proxy components similarly focus on stable algorithmic concepts and structural reasoning tokens. This case study suggests that the four components are not redundant and that direct and causal paths provide distinguishable valuation signals.

Additional robustness analyses. App. D.1 analyzes the Fisher-drift proxy; App. D.2 diagnoses the value-propagation approximation. Apps. D.3–D.5 provide token coverage, representation stability, and attribution analyses. Apps. D.6–D.9 report efficiency, additional dataset and baselines, preference-optimization ablations, and sensitivity.

6 Conclusion

We introduce AlphaToken, a response-token valuation framework for LLM post-training. AlphaToken decouples token value into two objectives, target adaptation and retention stability, and splits each objective along two paths by combining the direct signal with its downstream causal-path influence. As retention data are typically unavailable in practice, a Fisher-drift proxy anchored at the pre-trained reference replaces the inaccessible retention gradient, and a Ghost Dot-Product family extended to token-level computes all four scores at activation-space cost. Experiments on SFT and PO across 3B to 9B backbones confirm that AlphaToken improves the adaptation and retention trade-off while mitigating catastrophic forgetting.

Limitations

We discuss limitations. (i) Computational overhead. Under default $K=3$, $W=32$, and $B_{\text{val}}=32$, per-step overhead remains modest. Nevertheless, the scoring cost grows with the number of scored layers, causal window, and validation batch size, so K , W , and B_{val} may need re-budgeting for deeper models or longer contexts. (ii) Retention-proxy assumptions. The Fisher-drift proxy is tight when the reference checkpoint is near-stationary for inaccessible retention loss and the Fisher–Hessian mismatch is small. For under-trained or heavily domain-specialized checkpoints, residual and calibration gap may increase, making the proxy noisier. (iii) Hard masking. We instantiate AlphaToken with a binary top- ρ mask. Although this is simple and efficient, it discretizes continuous token values into hard keep/drop decisions. Soft reweighting, value-conditioned learning rates, and schedules over ρ are left to future work. We do not foresee ethical risks beyond those inherent to LLM adaptation.

References

Alvaro Bartolome, Gabriel Martin, and Daniel Vila. 2023. Notus. <https://github.com/argilla-io/notus>.

Samyadeep Basu, Phil Pope, and Soheil Feizi. 2021. Influence functions in deep learning are fragile. In *International Conference on Learning Representations*.

Mark Chen, Jerry Tworek, Heewoo Jun, Qiming Yuan, Henrique Ponde De Oliveira Pinto, Jared Kaplan, Harri Edwards, Yuri Burda, Nicholas Joseph, Greg

Brockman, and 1 others. 2021. Evaluating large language models trained on code. *arXiv preprint arXiv:2107.03374*.

Fenia Christopoulou, Ronald Cardenas, Gerasimos Lampouras, Haitham Bou-Ammar, and Jun Wang. 2024. Sparsepo: Controlling preference alignment of llms via sparse token masks. *arXiv preprint arXiv:2410.05102*.

Peter Clark, Isaac Cowhey, Oren Etzioni, Tushar Khot, Ashish Sabharwal, Carissa Schoenick, and Oyvind Tafjord. 2018. Think you have solved question answering? try arc, the ai2 reasoning challenge. *arXiv preprint arXiv:1803.05457*.

Karl Cobbe, Vineet Kosaraju, Mohammad Bavarian, Mark Chen, Heewoo Jun, Lukasz Kaiser, Matthias Plappert, Jerry Tworek, Jacob Hilton, Reiichiro Nakano, and 1 others. 2021. Training verifiers to solve math word problems. *arXiv preprint arXiv:2110.14168*.

Ning Ding, Yulin Chen, Bokai Xu, Yujia Qin, Shengding Hu, Zhiyuan Liu, Maosong Sun, and Bowen Zhou. 2023. Enhancing chat language models by scaling high-quality instructional conversations. In *Proceedings of the 2023 Conference on Empirical Methods in Natural Language Processing*, pages 3029–3051.

Amirata Ghorbani, Michael Kim, and James Zou. 2020. A distributional framework for data valuation. In *International Conference on Machine Learning*, pages 3535–3544. PMLR.

Amirata Ghorbani and James Zou. 2019. Data shapley: Equitable valuation of data for machine learning. In *International conference on machine learning*, pages 2242–2251. PMLR.

Aaron Grattafiori, Abhimanyu Dubey, and Abhinav Jauhri et al. 2024. *The llama 3 herd of models*. Preprint, arXiv:2407.21783.

Dan Hendrycks, Collin Burns, Steven Basart, Andy Zou, Mantas Mazeika, Dawn Song, and Jacob Steinhardt. 2021. Measuring massive multitask language understanding. In *International Conference on Learning Representations*.

Miriam Horovicz and Roni Goldshmidt. 2024. Token-shap: Interpreting large language models with monte carlo shapley value estimation. In *Proceedings of the 1st Workshop on NLP for Science (NLP4Science)*, pages 1–8.

Edward J Hu, Yelong Shen, Phillip Wallis, Zeyuan Allen-Zhu, Yuanzhi Li, Shean Wang, Lu Wang, Weizhu Chen, and 1 others. 2022. Lora: Low-rank adaptation of large language models. *ICLR*, 1(2):3.

Ruoxi Jia, David Dao, Boxin Wang, Frances Ann Hubis, Nezihe Merve Gurel, Bo Li, Ce Zhang, Costas Spanos, and Dawn Song. 2019a. Efficient

- task-specific data valuation for nearest neighbor algorithms. *Proceedings of the VLDB Endowment*, 12(11):1610–1623.
- Ruoxi Jia, David Dao, Boxin Wang, Frances Ann Hubis, Nick Hynes, Nezihe Merve Gürel, Bo Li, Ce Zhang, Dawn Song, and Costas J Spanos. 2019b. Towards efficient data valuation based on the shapley value. In *The 22nd international conference on artificial intelligence and statistics*, pages 1167–1176. PMLR.
- Krishnateja Killamsetty, Sivasubramanian Durga, Ganesh Ramakrishnan, Abir De, and Rishabh Iyer. 2021. Grad-match: Gradient matching based data subset selection for efficient deep model training. In *International Conference on Machine Learning*, pages 5464–5474. PMLR.
- James Kirkpatrick, Razvan Pascanu, Neil Rabinowitz, Joel Veness, Guillaume Desjardins, Andrei A Rusu, Kieran Milan, John Quan, Tiago Ramalho, Agnieszka Grabska-Barwinska, and 1 others. 2017. Overcoming catastrophic forgetting in neural networks. *Proceedings of the national academy of sciences*, 114(13):3521–3526.
- Pang Wei Koh and Percy Liang. 2017. Understanding black-box predictions via influence functions. In *International conference on machine learning*, pages 1885–1894. PMLR.
- Frederik Kunstner, Philipp Hennig, and Lukas Balles. 2019. Limitations of the empirical fisher approximation for natural gradient descent. *Advances in neural information processing systems*, 32.
- Yongchan Kwon and James Zou. 2022. Beta shapley: a unified and noise-reduced data valuation framework for machine learning. In *International Conference on Artificial Intelligence and Statistics*, pages 8780–8802. PMLR.
- Tue Le, Hoang Tran Vuong, Quyen Tran, Linh Ngo Van, Mehrtash Harandi, and Trung Le. 2025. Token-level self-play with importance-aware guidance for large language models. In *The Thirty-ninth Annual Conference on Neural Information Processing Systems*.
- Tianle Li, Wei-Lin Chiang, Evan Frick, Lisa Dunlap, Banghua Zhu, Joseph E. Gonzalez, and Ion Stoica. 2024. From live data to high-quality benchmarks: The Arena-Hard pipeline.
- Weida Li and Yaoliang Yu. 2023. Robust data valuation with weighted banzhaf values. *Advances in Neural Information Processing Systems*, 36:60349–60383.
- Xuechen Li, Tianyi Zhang, Yann Dubois, Rohan Taori, Ishaan Gulrajani, Carlos Guestrin, Percy Liang, and Tatsunori B. Hashimoto. 2023. AlpacaEval: An automatic evaluator of instruction-following models. https://github.com/tatsu-lab/alpaca_eval.
- Zhizhong Li and Derek Hoiem. 2017. Learning without forgetting. *IEEE transactions on pattern analysis and machine intelligence*, 40(12):2935–2947.
- Jiacheng Lin, Zhongruo Wang, Kun Qian, Tian Wang, Arvind Srinivasan, Hansi Zeng, Ruo Chen Jiao, Xie Zhou, Jiri Gesi, Dakuo Wang, Yufan Guo, Kai Zhong, Weiqi Zhang, sujay sanghavi, Changyou Chen, Hyokun Yun, and Lihong Li. 2026. **SFT doesn’t always hurt general capabilities: Revisiting domain-specific fine-tuning in LLMs**. In *The Fourteenth International Conference on Learning Representations*.
- Zhenghao Lin, Zhibin Gou, Yeyun Gong, Xiao Liu, Ruo Chen Xu, Chen Lin, Yujiu Yang, Jian Jiao, Nan Duan, Weizhu Chen, and 1 others. 2024. Not all tokens are what you need for pretraining. *Advances in Neural Information Processing Systems*, 37:29029–29063.
- Liangxin Liu, Xuebo Liu, Derek F Wong, Dongfang Li, Ziyi Wang, Baotian Hu, and Min Zhang. 2024. Selectit: Selective instruction tuning for llms via uncertainty-aware self-reflection. *Advances in Neural Information Processing Systems*, 37:97800–97825.
- Tao Liu, Taiqiang Wu, Runming Yang, Shaoning Sun, Junjie Wang, and Yujiu Yang. 2026. Profit: Leveraging high-value signals in sft via probability-guided token selection. *arXiv preprint arXiv:2601.09195*.
- James Martens. 2020. New insights and perspectives on the natural gradient method. *Journal of Machine Learning Research*, 21(146):1–76.
- Rory Mitchell, Joshua Cooper, Eibe Frank, and Geoffrey Holmes. 2022. Sampling permutations for shapley value estimation. *Journal of Machine Learning Research*, 23(43):1–46.
- Manish Nagaraj, Sakshi Choudhary, Utkarsh Saxena, Deepak Ravikumar, and Kaushik Roy. 2025. Trim: Token-wise attention-derived saliency for data-efficient instruction tuning. *arXiv preprint arXiv:2510.07118*.
- Elisa Nguyen, Minjoon Seo, and Seong Joon Oh. 2023. A bayesian approach to analysing training data attribution in deep learning. *Advances in Neural Information Processing Systems*, 36:64155–64180.
- Ramin Okhrati and Aldo Lipani. 2021. A multilinear sampling algorithm to estimate shapley values. In *2020 25th International Conference on Pattern Recognition (ICPR)*, pages 7992–7999. IEEE.
- Long Ouyang, Jeffrey Wu, Xu Jiang, Diogo Almeida, Carroll Wainwright, Pamela Mishkin, Chong Zhang, Sandhini Agarwal, Katarina Slama, Alex Ray, and 1 others. 2022. Training language models to follow instructions with human feedback. *Advances in neural information processing systems*, 35:27730–27744.
- Jinlong Pang, Na Di, Zhaowei Zhu, Jiaheng Wei, Hao Cheng, Chen Qian, and Yang Liu. 2025. Token cleaning: Fine-grained data selection for LLM supervised fine-tuning. In *Forty-second International Conference on Machine Learning*.

- Mansheej Paul, Surya Ganguli, and Gintare Karolina Dziugaite. 2021. Deep learning on a data diet: Finding important examples early in training. *Advances in neural information processing systems*, 34:20596–20607.
- Jincheng Peng, Huanlai Xing, Zhiwen Xiao, Lexi Xu, and Xianfu Lei. 2025. Large model empowered multi-modal semantic communication with selective tokens for training. *IEEE Signal Processing Letters*.
- Xiaohan Qin, Xiaoxing Wang, Ning Liao, Cancheng Zhang, Xiangdong Zhang, Mingquan Feng, Jingzhi Wang, and Junchi Yan. 2026. sstoken: Self-modulated and semantic-aware token selection for LLM fine-tuning. In *The Fourteenth International Conference on Learning Representations*.
- Qwen Team. 2026. Qwen3.5: Towards native multi-modal agents.
- Rafael Rafailov, Archit Sharma, Eric Mitchell, Christopher D Manning, Stefano Ermon, and Chelsea Finn. 2023. Direct preference optimization: Your language model is secretly a reward model. *Advances in neural information processing systems*, 36:53728–53741.
- Sunny Sanyal, Hayden Prairie, Rudrajit Das, Ali Kavis, and Sujay Sanghavi. 2025. Upweighting easy samples in fine-tuning mitigates forgetting. In *Forty-second International Conference on Machine Learning*.
- Xiaofeng Shi, Qian Kou, Yuduo Li, and Hua Zhou. 2025. Rethinking supervised fine-tuning: Emphasizing key answer tokens for improved llm accuracy. *arXiv preprint arXiv:2512.21017*.
- Antoine Simoulin, Namyong Park, Xiaoyi Liu, and Grey Yang. 2024. Memory-efficient fine-tuning of transformers via token selection. In *Proceedings of the 2024 Conference on Empirical Methods in Natural Language Processing*, pages 21565–21580.
- Gemma Team, Aishwarya Kamath, Johan Ferret, Shreya Pathak, Nino Vieillard, and Ramona Merhej et al. 2025. **Gemma 3 technical report**. *Preprint*, arXiv:2503.19786.
- Jiachen T Wang and Ruoxi Jia. 2023. Data banzhaf: A robust data valuation framework for machine learning. In *International conference on artificial intelligence and statistics*, pages 6388–6421. PMLR.
- Jiachen T. Wang, Prateek Mittal, Dawn Song, and Ruoxi Jia. 2025a. Data shapley in one training run. In *The Thirteenth International Conference on Learning Representations*.
- Jiachen T. Wang, Dawn Song, James Zou, Prateek Mittal, and Ruoxi Jia. 2025b. Capturing the temporal dependence of training data influence. In *The Thirteenth International Conference on Learning Representations*.
- Jiachen T Wang, Tong Wu, Dawn Song, Prateek Mittal, and Ruoxi Jia. 2024. Greats: Online selection of high-quality data for llm training in every iteration. *Advances in Neural Information Processing Systems*, 37:131197–131223.
- Shaobo Wang, Jiaming Wang, Jiajun Zhang, Cong Wang, Yue Min, Zichen Wen, Xingzhang Ren, Fei Huang, Huiqiang Jiang, Junyang Lin, and 1 others. 2025c. Winning the pruning gamble: A unified approach to joint sample and token pruning for efficient supervised fine-tuning. *arXiv preprint arXiv:2509.23873*.
- Tianhao Wang, Johannes Rausch, Ce Zhang, Ruoxi Jia, and Dawn Song. 2020. A principled approach to data valuation for federated learning. In *Federated Learning: Privacy and Incentive*, pages 153–167. Springer.
- Yuxiang Wei, Zhe Wang, Jiawei Liu, Yifeng Ding, and LINGMING ZHANG. 2024. Magicoder: Empowering code generation with OSS-instruct. In *Forty-first International Conference on Machine Learning*.
- Mitchell Wortsman, Gabriel Ilharco, Jong Wook Kim, Mike Li, Simon Kornblith, Rebecca Roelofs, Raphael Gontijo Lopes, Hannaneh Hajishirzi, Ali Farhadi, Hongseok Namkoong, and Ludwig Schmidt. 2022. Robust fine-tuning of zero-shot models. In *Proceedings of the IEEE/CVF Conference on Computer Vision and Pattern Recognition (CVPR)*, pages 7959–7971.
- Chao-Chung Wu, Zhi Rui Tam, Chieh-Yen Lin, Yun-Nung Chen, Shao-Hua Sun, and Hung yi Lee. 2025. Mitigating forgetting in LLM fine-tuning via low-perplexity token learning. In *The Thirty-ninth Annual Conference on Neural Information Processing Systems*.
- Mengzhou Xia, Sadhika Malladi, Suchin Gururangan, Sanjeev Arora, and Danqi Chen. 2024. LESS: Selecting influential data for targeted instruction tuning. In *Forty-first International Conference on Machine Learning*.
- Yingtai Xiao, Yuqing Zhu, Sirat Samyoun, Wanrong Zhang, Jiachen T Wang, and Jian Du. 2025. Token-shapley: Token level context attribution with shapley value. In *Findings of the Association for Computational Linguistics: ACL 2025*, pages 3882–3894.
- Jie Xu, Zihan Wu, Cong Wang, and Xiaohua Jia. 2025. Liveval: Real-time and trajectory-based data valuation via adaptive reference points. In *Proceedings of the 34th ACM International Conference on Information and Knowledge Management*, pages 3623–3634.
- Kailai Yang, Zhiwei Liu, Qianqian Xie, Jimin Huang, Erxue Min, and Sophia Ananiadou. 2025. Selective preference optimization via token-level reward function estimation. In *Proceedings of the 2025 Conference on Empirical Methods in Natural Language Processing*, pages 7043–7067.

Ning Yang, Hai Lin, Yibo Liu, Baoliang Tian, Guoqing Liu, and Haijun Zhang. 2026a. Token-importance guided direct preference optimization. In *The Fourteenth International Conference on Learning Representations*.

Yuchen Yang, Wenze Lin, Enhao Huang, Zhixuan Chu, Hongbin Zhou, Lan Tao, Yiming Li, Zhan Qin, and Kui Ren. 2026b. Explainable token-level noise filtering for LLM fine-tuning datasets. In *The Fourteenth International Conference on Learning Representations*.

Hee Suk Yoon, Eunseop Yoon, Mark A. Hasegawa-Johnson, Sungwoong Kim, and Chang D. Yoo. 2025. ConfPO: Exploiting policy model confidence for critical token selection in preference optimization. In *Forty-second International Conference on Machine Learning*.

Rowan Zellers, Ari Holtzman, Yonatan Bisk, Ali Farhadi, and Yejin Choi. 2019. Hellaswag: Can a machine really finish your sentence? In *Proceedings of the 57th annual meeting of the association for computational linguistics*, pages 4791–4800.

A Token Valuation via In-Run Shapley from an Optimal Masking View

Setup: fine-tuning as optimal masking. We reframe token-level data selection as an optimal masking problem that controls which token-level losses contribute gradients during optimization, a perspective shared by selective training and pruning schemes for LLM adaptation (Simoulin et al., 2024; Pang et al., 2025; Wu et al., 2025). Let $\mathcal{D}_{\text{train}} = \{(\mathbf{x}^{(i)}, \mathbf{y}^{(i)})\}$ be the training corpus with response $\mathbf{y}^{(i)} = [y_1^{(i)}, \dots, y_{T_i}^{(i)}]$. We attach a binary mask $\mathbf{m}^{(i)} \in \{0, 1\}^{T_i}$ indicating whether token $y_t^{(i)}$ contributes to the gradient. The collection $\mathbf{M} = \{\mathbf{m}^{(i)}\}$ instantiates token selection as a discrete control variable. The goal is an optimal \mathbf{M}^* minimizing a validation loss \mathcal{L}_{val} on a held-out set $\mathcal{D}_{\text{val}} = \{(\mathbf{x}_0, \mathbf{y}_0)\}$:

$$\min_{\mathbf{M}} \mathcal{L}_{\text{val}}(\mathbf{x}_0, \mathbf{y}_0; \boldsymbol{\theta}^*), \quad (15)$$

$$\text{s.t. } \boldsymbol{\theta}^* = \arg \min_{\boldsymbol{\theta}} \sum_{i \in \mathcal{D}_{\text{train}}} \mathcal{L}(\mathbf{x}^{(i)}, \mathbf{y}^{(i)} \odot \mathbf{m}^{(i)}; \boldsymbol{\theta}). \quad (16)$$

Here $\mathbf{y}^{(i)} \odot \mathbf{m}^{(i)}$ implies the loss is computed only on unmasked positions, equivalently, masked tokens contribute zero gradient—a selective back-propagation that reallocates compute toward high-value signals (Simoulin et al., 2024). This is a token-level analogue of example reweighting and subset selection (Paul et al., 2021; Killamsetty et al., 2021).

Token-player utility. For each example $(\mathbf{x}^{(i)}, \mathbf{y}^{(i)})$ define token *players* $u = (i, t)$ with token-level loss $\ell_u(\boldsymbol{\theta})$ (e.g., teacher-forced negative log-likelihood). Following the Data Shapley convention, we take the to-be-maximised global utility to be the negative validation loss of the trained model,

$$\mathcal{U}(\mathbf{M}) := -\mathcal{L}_{\text{val}}(\mathbf{x}_0, \mathbf{y}_0; \boldsymbol{\theta}^*(\mathbf{M})). \quad (17)$$

Exact token-level Shapley values under \mathcal{U} are computationally prohibitive because the per-sequence player count is large (Ghorbani and Zou, 2019), motivating an in-run surrogate.

In-run local utility along a single trajectory. Following Wang et al. (2025a), we replace $\mathcal{U}(\mathbf{M})$ by a sum of *local* utilities along one optimization trajectory. Let $\boldsymbol{\theta}_s$ be the parameters at iteration s , \mathcal{B}_s the player set induced by the minibatch, and

$S_s \subseteq \mathcal{B}_s$ the retained subset. The masked one-step update is

$$\boldsymbol{\theta}_{s+1}(S_s) = \boldsymbol{\theta}_s - \eta_s \sum_{u \in S_s} \nabla_{\boldsymbol{\theta}} \ell_u(\boldsymbol{\theta}_s), \quad (18)$$

and the local utility is the induced validation-loss decrease,

$$\Delta_s(S_s) := \mathcal{L}_{\text{val}}(\boldsymbol{\theta}_s) - \mathcal{L}_{\text{val}}(\boldsymbol{\theta}_{s+1}(S_s)). \quad (19)$$

The global effect of token retention is approximated by accumulating Δ_s across steps.

Closed-form token value via first-order linearization. A first-order Taylor expansion of $\mathcal{L}_{\text{val}}(\boldsymbol{\theta}_{s+1}(S_s))$ around $\boldsymbol{\theta}_s$ gives

$$\begin{aligned} \Delta_s(S_s) &\approx -\nabla_{\boldsymbol{\theta}} \mathcal{L}_{\text{val}}(\boldsymbol{\theta}_s)^\top (\boldsymbol{\theta}_{s+1}(S_s) - \boldsymbol{\theta}_s) \\ &= \eta_s \sum_{u \in S_s} \langle \nabla_{\boldsymbol{\theta}} \mathcal{L}_{\text{val}}(\boldsymbol{\theta}_s), \nabla_{\boldsymbol{\theta}} \ell_u(\boldsymbol{\theta}_s) \rangle. \end{aligned} \quad (20)$$

Since $\widehat{\Delta}_s(S_s) = \eta_s \sum_{u \in S_s} a_{u,s}$ is additive in S_s , the Shapley value of player u at step s collapses to its individual contribution,

$$\phi_{u,s} = \eta_s \langle \nabla_{\boldsymbol{\theta}} \mathcal{L}_{\text{val}}(\boldsymbol{\theta}_s), \nabla_{\boldsymbol{\theta}} \ell_u(\boldsymbol{\theta}_s) \rangle. \quad (21)$$

Within a single training step η_s is shared across tokens and absorbed into the threshold τ_ρ ; we therefore drop it from the main-text $\Phi(y_t)$ formula. Accumulating across steps, when desired, would simply weight steps by η_s .

Alignment–stability decomposition. AlphaToKen uses a composite validation objective

$$\mathcal{L}_{\text{val}}(\boldsymbol{\theta}) = \mathcal{L}_{\text{align}}(\boldsymbol{\theta}) + \lambda \mathcal{L}_{\text{stab}}(\boldsymbol{\theta}), \quad (22)$$

with $\mathcal{L}_{\text{align}}$ encoding target-task (or preference) utility and $\mathcal{L}_{\text{stab}}$ encoding retention/stability. By inner-product linearity, Eq. (21) decomposes as

$$\begin{aligned} \phi_{u,s} &= \eta_s \langle \nabla \mathcal{L}_{\text{align}}(\boldsymbol{\theta}_s), \nabla \ell_u(\boldsymbol{\theta}_s) \rangle \\ &\quad + \eta_s \lambda \langle \nabla \mathcal{L}_{\text{stab}}(\boldsymbol{\theta}_s), \nabla \ell_u(\boldsymbol{\theta}_s) \rangle. \end{aligned} \quad (23)$$

When retention validation data are unavailable, $\mathcal{L}_{\text{stab}}$ may be replaced by any differentiable proxy; the derivation only requires $\nabla \mathcal{L}_{\text{stab}}$ to be computable.

Autoregressive downstream influence. Replacing ℓ_u with an augmented term $\tilde{\ell}_u$ whose gradient aggregates the position- t direct contribution and the propagation to later positions preserves additivity, so Eq. (21) generalises to $\phi_{u,s} = \eta_s \langle \nabla \mathcal{L}_{\text{val}}, \nabla \tilde{\ell}_u \rangle$, unifying immediate learning benefit and downstream predictive influence within the same in-run Shapley framework.

Position relative to prior work. Eqs. (15)–(16) expose existing token-level methods as *restricted families* of masks: low-perplexity token learning constrains $m^{(i)}$ via perplexity profiles (Wu et al., 2025); Token Cleaning uses token-wise loss disparity (Pang et al., 2025); explainable filtering applies novelty/reasoning priors (Yang et al., 2026b); SePO, TI-DPO, and ConfPO impose token masks or weights to modulate preference gradients (Christopoulou et al., 2024; Yang et al., 2026a; Yoon et al., 2025). These designs each optimize a single proxy signal and are not derived as objective-aligned solutions to \mathcal{L}_{val} , leaving systematic control of plasticity vs. stability ad hoc (Kirkpatrick et al., 2017; Li and Hoiem, 2017). Our derivation supplies the missing link.

B Theoretical Analysis

This appendix consolidates every derivation and proof deferred from the main text. We organise the material into four parts. App. B.1 sets up the causal gradient decomposition, derives the analytical form of the cross-position Jacobian, and proves universality across SFT and DPO. App. B.2 establishes the three GDP factorizations. App. B.3 gives the complete proof of the Value-Propagation approximation bound. App. B.4 gives the complete proof of the retention proxy bound, including a fine-grained decomposition of the Fisher–Hessian gap. Notation matches Sec. 3 and Sec. 4.

B.1 Causal Gradient Decomposition

B.1.1 Notation

A decoder-only Transformer is parameterised by $\boldsymbol{\theta} = \{\boldsymbol{\theta}^l\}_{l=1}^L$. For input \boldsymbol{x} and length- T response \boldsymbol{y} , the layer- l hidden state at position t is $\boldsymbol{h}_t^l \in \mathbb{R}^d$, with $\boldsymbol{h}_t^{(0)}$ the input embedding. The training objective factorizes as $\mathcal{L}(\boldsymbol{\theta}) = \sum_{k=1}^T \ell_k(\boldsymbol{\theta})$. Causal masking enforces that \boldsymbol{h}_k^l depends strictly on $\{\boldsymbol{h}_i^{l-1}\}_{i \leq k}$, so any token y_t enters \mathcal{L} both *directly* via ℓ_t and *indirectly* via every ℓ_k with $k > t$.

B.1.2 Direct and Causal Components

Define $\nabla_{\boldsymbol{\theta}} \mathcal{L}_t^{\text{tot}}$ as the gradient component causally attributable to position t through the immediate self-term and the single-hop cross-position transfer. Routing each future loss ℓ_k ($k > t$) backward through the layer- l attention transfer $\boldsymbol{J}_{k,t}^l$ and isolating the self-term $k=t$ yields

$$\nabla_{\boldsymbol{\theta}} \mathcal{L}_t^{\text{tot}} = \nabla_{\boldsymbol{\theta}} \ell_t + \sum_{k=t+1}^T \sum_{l=1}^L \delta_k^l \boldsymbol{J}_{k,t}^l \boldsymbol{\Theta}_t^{l-1}. \quad (24)$$

with $\delta_k^l \triangleq \partial \ell_k / \partial \mathbf{h}_k^l \in \mathbb{R}^{1 \times d}$, $\mathbf{J}_{k,t}^l \triangleq \partial \mathbf{h}_k^l / \partial \mathbf{h}_t^{l-1}$, and $\Theta_t^{l-1} \triangleq \partial \mathbf{h}_t^{l-1} / \partial \theta$. Eq. (24) reproduces Eq. (3). Each additional cross-position hop introduces one further Jacobian factor $\mathbf{J}_{k,t}^l$, so an m -hop path decays as $O(d_h^{-m/2})$ in the score-propagation component (App. B.3); the single-hop transfer is the dominant channel under saturated and sparse attention regimes.

B.1.3 Cross-Position Jacobian

At layer l , attention projects \mathbf{h}^{l-1} via $\mathbf{W}_Q^l, \mathbf{W}_K^l, \mathbf{W}_V^l$, producing weights $\alpha_{k,i}^l = \text{softmax}_i(\mathbf{q}_k^l(\mathbf{k}_i^l)^\top / \sqrt{d_h})$ and output $\mathbf{o}_k^l = \sum_{i \leq k} \alpha_{k,i}^l \mathbf{v}_i^l$. Differentiating \mathbf{o}_k^l w.r.t. \mathbf{h}_t^{l-1} for $t < k$ separates two channels:

$$\frac{\partial \mathbf{o}_k^l}{\partial \mathbf{h}_t^{l-1}} = \underbrace{\alpha_{k,t}^l \mathbf{W}_V^l}_{\text{Value-Propagation}} + \underbrace{\sum_{i \leq k} \frac{\partial \alpha_{k,i}^l}{\partial \mathbf{h}_t^{l-1}} \otimes \mathbf{v}_i^l}_{\text{Score-Propagation}}. \quad (25)$$

Applying $\partial \alpha_{k,i}^l / \partial e_{k,t}^l = \alpha_{k,i}^l (\delta_{it} - \alpha_{k,t}^l)$ with $e_{k,t}^l = \mathbf{q}_k^l(\mathbf{k}_t^l)^\top / \sqrt{d_h}$ collapses the Score-Propagation to

$$\text{Path}_{\text{Score}} = \frac{\alpha_{k,t}^l}{\sqrt{d_h}} (\mathbf{v}_t^l - \mathbf{o}_k^l) \otimes (\mathbf{q}_k^l(\mathbf{W}_K^l)^\top). \quad (26)$$

Combining,

$$\mathbf{J}_{k,t}^l = \alpha_{k,t}^l \mathbf{W}_V^l + \frac{\alpha_{k,t}^l}{\sqrt{d_h}} (\mathbf{v}_t^l - \mathbf{o}_k^l) \otimes (\mathbf{q}_k^l(\mathbf{W}_K^l)^\top), \quad (27)$$

where the Score-Propagation inherits a $1/\sqrt{d_h}$ attenuation directly from dot-product attention, justifying the Value-Propagation approximation in App. B.3.

B.1.4 Universality across SFT and DPO

Eq. (24) is independent of the choice of ℓ_k .

SFT. With $\mathcal{L}_{\text{SFT}} = \sum_k \ell_k$ and $\ell_k = -\log \pi_\theta(y_k | \mathbf{x}, \mathbf{y}_{<k})$, summing Eq. (24) over t trivially recovers $\nabla_\theta \mathcal{L}_{\text{SFT}} = \sum_t \nabla_\theta \ell_t^{\text{tot}}$.

DPO. The sequence-level objective $\mathcal{L}_{\text{DPO}} = -\log \sigma(s)$ unrolls via $\nabla_s[-\log \sigma(s)] = -\sigma(-s)$ into per-position pseudo-losses $\ell_k^\pm = \pm \omega(-\log \pi_\theta(y_k^\pm | \mathbf{x}, \mathbf{y}_{<k}^\pm))$ with $\omega \triangleq \beta \sigma(-s)$. Define the formal token-routing notation

$$\nabla_\theta \ell_k^+ |_{\text{via } t} \triangleq \sum_{l=1}^L \delta_k^l \mathbf{J}_{k,t}^l \Theta_t^{l-1}, \quad (28)$$

i.e., the contribution of ℓ_k^+ that backpropagates through position t 's hidden state at layer l . In a

causal LM, $\nabla_\theta \ell_k^+ = \sum_{t \leq k} \nabla_\theta \ell_k^+ |_{\text{via } t}$. Substituting and swapping the order of summation,

$$\sum_{k=1}^{|y^+|} \sum_{t=1}^k \nabla_\theta \ell_k^+ |_{\text{via } t} = \sum_{t=1}^{|y^+|} \left(\nabla_\theta \ell_t^+ |_{\text{via } t} + \sum_{k=t+1}^{|y^+|} \nabla_\theta \ell_k^+ |_{\text{via } t} \right). \quad (29)$$

The summand inside the parenthesis matches Eq. (24) term-for-term; the rejected branch follows symmetrically with the sign of ω reversed.

B.2 Ghost Dot-Product Factorizations

We prove the three GDP identities used in Sec. 3.4. Two elementary facts: every token-level linear-layer gradient is rank-1,

$$\nabla_{\mathbf{W}^l} \ell_t = \delta_t^l \otimes \mathbf{h}_t^l; \quad (30)$$

and the Frobenius inner product of two rank-1 tensors decouples,

$$\langle \mathbf{u} \otimes \mathbf{v}, \mathbf{u}' \otimes \mathbf{v}' \rangle_F = \langle \mathbf{u}, \mathbf{u}' \rangle \langle \mathbf{v}, \mathbf{v}' \rangle. \quad (31)$$

We never materialize full parameter gradients in any of the three forms below.

B.2.1 Direct Token Alignment (A–A)

For each validation token $v \in \mathcal{V}_{\text{tgt}}$, the per-token gradient $\nabla_{\mathbf{W}^l} \ell_v = \delta_v^l \otimes \mathbf{h}_v^l$ is rank-1, so applying Eq. (31) to Eq. (30) gives

$$\langle \nabla_{\mathbf{W}^l} \ell_t, \nabla_{\mathbf{W}^l} \ell_v \rangle_F = \langle \delta_t^l, \delta_v^l \rangle \langle \mathbf{h}_t^l, \mathbf{h}_v^l \rangle. \quad (32)$$

Averaging over \mathcal{V}_{tgt} keeps the score scale invariant to validation batch size; summing further over l yields $\Phi_{\text{tgt}}^{\text{dir}}(y_t)$. This A–A factorization follows the construction of Wang et al. (2025a).

B.2.2 Causal Token Alignment (A–A causal)

Under the Value-Propagation approximation $\hat{\mathbf{J}}_{k,t}^l = \alpha_{t \rightarrow k}^l \mathbf{W}_V^l$, where $\alpha_{t \rightarrow k}^l \equiv \alpha_{k,t}^l$, the cross-position contribution becomes rank-1 in the value-projection parameters,

$$\nabla_{\mathbf{W}_V^l} \ell_{t \rightarrow k} \approx \alpha_{t \rightarrow k}^l (\delta_k^l \otimes \mathbf{h}_t^{l-1}), \quad (33)$$

with the shorthand $\alpha_{t \rightarrow k}^l \equiv \alpha_{k,t}^l$. For each validation token $v \in \mathcal{V}_{\text{tgt}}$, applying Eq. (31) once more gives

$$\langle \nabla_{\mathbf{W}_V^l} \ell_{t \rightarrow k}, \nabla_{\mathbf{W}_V^l} \ell_v \rangle_F \approx \alpha_{t \rightarrow k}^l \langle \delta_k^l, \delta_v^l \rangle \langle \mathbf{h}_t^{l-1}, \mathbf{h}_v^{l-1} \rangle. \quad (34)$$

Averaging this quantity over $v \in \mathcal{V}_{\text{tgt}}$ and summing over $l \in \mathcal{S}$ and future positions k yields $\Phi_{\text{tgt}}^{\text{cau}}(y_t)$.

B.2.3 Activation–Parameter GDP for the Retention Proxy (A–P)

The retention proxy $\mathbf{g}_{\text{prx}} = \mathbf{F}_{\text{ref}}(\boldsymbol{\theta} - \boldsymbol{\theta}_{\text{ref}})$ is a fixed parameter-space vector and is *not* the back-propagated output of any sample-level loss; it cannot be expressed as $\delta_{\text{val}} \otimes \mathbf{h}_{\text{val}}$, so Eq. (31) does not apply. We exploit only the rank-1 form Eq. (30) of the token gradient. Writing $\mathbf{V}^l \triangleq \mathbf{F}_{\mathbf{W}^l} \odot (\mathbf{W}^l - \mathbf{W}_{\text{ref}}^l)$, where $\mathbf{F}_{\mathbf{W}^l} \triangleq \text{Diag}(\mathbf{F}_{\text{ref}})|_{\mathbf{W}^l}$ is the layer- l slice of the diagonal Fisher (refreshed once per training step), and using the trace identity $\langle \mathbf{u} \otimes \mathbf{v}, \mathbf{M} \rangle_F = \mathbf{u}^\top \mathbf{M} \mathbf{v}$,

$$\langle \nabla_{\mathbf{W}^l} \ell_t, \mathbf{V}^l \rangle_F = (\delta_t^l)^\top \mathbf{V}^l \mathbf{h}_t^l. \quad (35)$$

Stacking activations for T tokens into $\mathbf{H}^l \in \mathbb{R}^{T \times d_{\text{in}}}$ and errors into $\boldsymbol{\Delta}^l \in \mathbb{R}^{T \times d_{\text{out}}}$, all T scores collapse to one GEMM $\mathbf{H}^l (\mathbf{V}^l)^\top \in \mathbb{R}^{T \times d_{\text{out}}}$, followed by an element-wise product with $\boldsymbol{\Delta}^l$ and summation over the output dimension, with complexity $\mathcal{O}(T d_{\text{in}} d_{\text{out}})$. We apply this factorization to all linear layers in attention and MLP blocks; embedding and lm_head layers are excluded from the scoring layer set \mathcal{S} . For LoRA-adapted layers, $\mathbf{F}_{\mathbf{W}^l}$ is computed and contracted on the LoRA factors A, B separately; the cache is small. The same construction with $\alpha_{t \rightarrow k}^l \delta_k^l$ and \mathbf{h}_t^{l-1} gives the causal proxy term analogously to Eq. (34).

B.3 Value-Propagation Approximation Bound

We prove the bound on the residual between the exact cross-position Jacobian and its Value-Propagation approximation $\hat{\mathbf{J}}_{k,t}^l = \alpha_{t \rightarrow k}^l \mathbf{W}_{V}^l$. From Eq. (27), the residual equals the Score-Propagation component exactly:

$$\mathcal{R}_{\text{score}} \triangleq \mathbf{J}_{k,t}^l - \hat{\mathbf{J}}_{k,t}^l = \frac{\alpha_{t \rightarrow k}^l}{\sqrt{d_h}} (\mathbf{v}_t - \mathbf{o}_k^l) \otimes (\mathbf{q}_k^l (\mathbf{W}_K^l)^\top), \quad (36)$$

where $\alpha_{t \rightarrow k}^l \equiv \alpha_{k,t}^l \in [0, 1]$ denotes the scalar attention weight by which future position k attends to source position t .

Operator-norm bound. For any rank-1 outer product, $\|\mathbf{u} \otimes \mathbf{v}\|_{\text{op}} = \|\mathbf{u}\|_2 \|\mathbf{v}\|_2$. Applying this to Eq. (36) and bounding $\|\mathbf{q}_k^l (\mathbf{W}_K^l)^\top\|_2 \leq \|\mathbf{q}_k^l\|_2 \|\mathbf{W}_K^l\|_{\text{op}}$,

$$\|\mathcal{R}_{\text{score}}\|_{\text{op}} \leq \frac{\alpha_{t \rightarrow k}^l}{\sqrt{d_h}} \|\mathbf{v}_t - \mathbf{o}_k^l\|_2 \|\mathbf{q}_k^l\|_2 \|\mathbf{W}_K^l\|_{\text{op}}. \quad (37)$$

Letting $Q \triangleq \sup_{k,l} \|\mathbf{q}_k^l\|_2$ and $C \triangleq Q \|\mathbf{W}_K^l\|_{\text{op}}$, both finite for any well-defined Transformer,

$$\|\mathcal{R}_{\text{score}}\|_{\text{op}} \leq \frac{C}{\sqrt{d_h}} \alpha_{t \rightarrow k}^l \|\mathbf{v}_t - \mathbf{o}_k^l\|_2. \quad (38)$$

Saturation analysis. Eq. (38) vanishes at *both* extremes of the attention regime:

- *Sparse attention* ($\alpha_{t \rightarrow k}^l \rightarrow 0$): the prefactor drives the residual to zero directly.
- *Saturated attention* ($\alpha_{t \rightarrow k}^l \rightarrow 1$): the output $\mathbf{o}_k^l = \sum_i \alpha_{k,i}^l \mathbf{v}_i^l$ collapses to \mathbf{v}_t^l , so $\|\mathbf{v}_t^l - \mathbf{o}_k^l\|_2 \rightarrow 0$.

Combined with $\mathcal{O}(1/\sqrt{d_h})$, this proves $\mathcal{R}_{\text{score}}$ is small in both regimes. An empirical verification is given in App. D.2.

B.4 Fisher Drift Proxy without Retention Data

We prove the data-free retention proxy bound and decompose its Fisher–Hessian-gap term into individually controllable pieces. Let $\mathcal{L}_{\text{ret}}(\boldsymbol{\theta}) \triangleq \mathbb{E}_{(\mathbf{x}, \mathbf{y}) \sim \mathcal{D}_{\text{ret}}}[-\log p_{\boldsymbol{\theta}}(\mathbf{y}|\mathbf{x})]$ be the unobserved retention loss, and define

$$\mathbf{g}_{\text{ideal}} \triangleq \nabla_{\boldsymbol{\theta}} \mathcal{L}_{\text{ret}}(\boldsymbol{\theta}), \quad \mathbf{g}_{\text{prx}} \triangleq \mathbf{F}_{\text{ref}}(\boldsymbol{\theta} - \boldsymbol{\theta}_{\text{ref}}), \quad (39)$$

with \mathbf{F}_{ref} the Monte-Carlo Fisher of Sec. 3.3. Our goal is a bound on $\|\mathbf{g}_{\text{ideal}} - \mathbf{g}_{\text{prx}}\|$ that never evaluates expectations on \mathcal{D}_{ret} .

B.4.1 Second-Order Taylor Expansion

Assume $\mathcal{L}_{\text{ret}} \in C^3$ on a neighbourhood containing both $\boldsymbol{\theta}_{\text{ref}}$ and $\boldsymbol{\theta}$, and let $\Delta\boldsymbol{\theta} \triangleq \boldsymbol{\theta} - \boldsymbol{\theta}_{\text{ref}}$. Taylor’s theorem with mean-value remainder gives

$$\mathbf{g}_{\text{ideal}} = \mathbf{r}_0 + \mathbf{H}_{\text{ret}} \Delta\boldsymbol{\theta} + \frac{1}{2} \nabla^3 \mathcal{L}_{\text{ret}}(\boldsymbol{\xi}) [\Delta\boldsymbol{\theta}, \Delta\boldsymbol{\theta}], \quad (40)$$

for some $\boldsymbol{\xi} \in [\boldsymbol{\theta}_{\text{ref}}, \boldsymbol{\theta}]$, where $\mathbf{r}_0 \triangleq \nabla \mathcal{L}_{\text{ret}}(\boldsymbol{\theta}_{\text{ref}})$ and $\mathbf{H}_{\text{ret}} \triangleq \nabla^2 \mathcal{L}_{\text{ret}}(\boldsymbol{\theta}_{\text{ref}})$. Subtracting $\mathbf{g}_{\text{prx}} = \mathbf{F}_{\text{ref}} \Delta\boldsymbol{\theta}$ and applying the triangle inequality,

$$\|\mathbf{g}_{\text{ideal}} - \mathbf{g}_{\text{prx}}\| \leq \|\mathbf{r}_0\| + \|\mathbf{H}_{\text{ret}} - \mathbf{F}_{\text{ref}}\| \cdot \|\Delta\boldsymbol{\theta}\| + \frac{M_3}{2} \|\Delta\boldsymbol{\theta}\|^2, \quad (41)$$

where $M_3 \triangleq \sup_{\boldsymbol{\xi} \in [\boldsymbol{\theta}_{\text{ref}}, \boldsymbol{\theta}]} \|\nabla^3 \mathcal{L}_{\text{ret}}(\boldsymbol{\xi})\|_{\text{op}}$.

Remark on $\|\mathbf{r}_0\|$. The retention loss is defined over a (potentially heterogeneous) collection of downstream tasks, and pre-training is performed on a different, language-modelling distribution. We therefore do *not* claim $\|\mathbf{r}_0\| = 0$; rather, $\|\mathbf{r}_0\|$ is small to the extent that retention performance inherits the pre-training optimum, and is upper-bounded empirically by measuring the gradient norm of the reference checkpoint on a held-out probe.

B.4.2 Decomposing the Fisher–Hessian Gap

As \mathbf{F}_{ref} is diagonal by construction (Sec. 3.3), we decompose $\|\mathbf{H}_{\text{ret}} - \mathbf{F}_{\text{ref}}\|$ into a diagonalisation residual, a calibration gap, and a Fisher transfer

error. We introduce the auxiliary *diagonal retention Fisher*

$$\mathbf{F}_{\text{ret}}^\dagger \triangleq \text{Diag}\left(\mathbb{E}_{\mathbf{x} \sim \mathcal{D}_{\text{ret}}, \tilde{\mathbf{y}} \sim p_{\theta_{\text{ref}}}(\cdot|\mathbf{x})}[\nabla_{\theta} \log p_{\theta_{\text{ref}}}(\tilde{\mathbf{y}}|\mathbf{x})^{\odot 2}]\right), \quad (42)$$

which uses retention prompts but model-sampled labels and serves purely as an analytical object. By the triangle inequality,

$$\|\mathbf{H}_{\text{ret}} - \mathbf{F}_{\text{ref}}\| \leq \underbrace{\|\mathbf{H}_{\text{ret}} - \text{Diag}(\mathbf{H}_{\text{ret}})\|}_{\Delta_{\text{off}}} + \underbrace{\|\text{Diag}(\mathbf{H}_{\text{ret}}) - \mathbf{F}_{\text{ret}}^\dagger\|}_{\Delta_{\text{cal}}} + \underbrace{\|\mathbf{F}_{\text{ret}}^\dagger - \mathbf{F}_{\text{ref}}\|}_{\text{Fisher transfer}}.$$

Diagonalisation residual Δ_{off} . This term captures the off-diagonal mass of \mathbf{H}_{ret} and reflects the standard diagonal-Fisher modeling choice adopted by EWC (Kirkpatrick et al., 2017) and related methods. It depends only on the local curvature of \mathcal{L}_{ret} at θ_{ref} and is independent of the input distribution used to construct \mathbf{F}_{ref} . Since $\mathbf{g}_{\text{prx}} = \mathbf{F}_{\text{ref}}\Delta\theta$ acts only through the diagonal subspace, Δ_{off} is absorbed multiplicatively by $\|\Delta\theta\|$, which value-aware masking actively keeps small throughout training.

Calibration gap Δ_{cal} . Under the maximum-likelihood condition—i.e., when $p_{\theta_{\text{ref}}}(\mathbf{y}|\mathbf{x})$ matches the conditional law of \mathcal{D}_{ret} —the Fisher information equals the negative log-likelihood Hessian (Martens, 2020), yielding $\mathbf{F}_{\text{ret}}^\dagger = \text{Diag}(\mathbf{H}_{\text{ret}})$ and $\Delta_{\text{cal}} = 0$. For a publicly released checkpoint, Δ_{cal} is upper-bounded by the residual KL divergence between the model’s predictive distribution and the data-generating conditional, which is small for well-calibrated pre-trained models.

Fisher transfer error. Both $\mathbf{F}_{\text{ret}}^\dagger$ and \mathbf{F}_{ref} evaluate at the same θ_{ref} and use labels drawn from the same conditional $p_{\theta_{\text{ref}}}(\cdot|\mathbf{x})$; they differ only in the input distribution. Letting L_g be the Lipschitz constant of the map $\mathbf{x} \mapsto \text{Diag}(\mathbb{E}_{\tilde{\mathbf{y}} \sim p_{\theta_{\text{ref}}}(\cdot|\mathbf{x})}[\nabla_{\theta} \log p_{\theta_{\text{ref}}}(\tilde{\mathbf{y}}|\mathbf{x})^{\odot 2}])$,

$$\|\mathbf{F}_{\text{ret}}^\dagger - \mathbf{F}_{\text{ref}}\| \leq L_g \mathcal{W}_2(p_{\mathcal{D}_{\text{ret}}}(\mathbf{x}), p_{\mathcal{X}}(\mathbf{x})). \quad (43)$$

This bound depends only on the linguistic representativeness of \mathcal{X} . Reusing \mathcal{D}_{tgt} prompts as \mathcal{X} keeps the Wasserstein distance small in practice, as both share the surface morphology of natural language.

B.4.3 Final Bound and Data-Free Reliability

Combining the residual, Fisher–Hessian mismatch, diagonalization, and higher-order terms, we obtain

$$\|\mathbf{g}_{\text{ideal}} - \mathbf{g}_{\text{prx}}\| \leq \|\mathbf{r}_0\| + (\Delta_{\text{off}} + \Delta_{\text{cal}} + L_g \mathcal{W}_2) \cdot \|\Delta\theta\| + \frac{M_3}{2} \|\Delta\theta\|^2.$$

Each of $\{\|\mathbf{r}_0\|, \Delta_{\text{cal}}, L_g \mathcal{W}_2, M_3\}$ is controlled under conditions our framework already enforces or that public checkpoints already satisfy, while the diagonalisation residual Δ_{off} follows the standard diagonal-Fisher modeling choice and is absorbed multiplicatively through $\|\Delta\theta\|$, which value-aware masking keeps small throughout training. The decomposition introduces \mathcal{D}_{ret} only as an analytical object for bounding the approximation error—AlphaToken never evaluates these expectations or accesses retention examples during training, and only uses \mathbf{F}_{ref} constructed from \mathcal{X} .

C Experiment Details

C.1 Baseline Details

We compare AlphaToken with representative baselines for supervised fine-tuning and preference optimization.

Supervised fine-tuning baselines. For SFT, we compare against full fine-tuning, parameter-efficient tuning, sample selection, token selection, and forgetting-resistant methods.

- **Pre-trained:** The original backbone before target-task fine-tuning, used as the reference point for measuring adaptation and forgetting.
- **Standard FT:** Full-parameter fine-tuning with the standard response-token cross-entropy loss.
- **LoRA (Hu et al., 2022):** A parameter-efficient baseline that freezes the backbone and updates low-rank adapter parameters.
- **LESS (Xia et al., 2024):** A sample-level selection baseline that selects training examples by gradient similarity to a target validation set.
- **Token Cleaning (Pang et al., 2025):** A token-filtering baseline that masks low-quality tokens using token-wise loss-discrepancy signals.
- **STM (Wu et al., 2025):** A token-masking baseline that selects response tokens according to local likelihood or perplexity-based statistics to mitigate forgetting.
- **XTF (Yang et al., 2026b):** An explainable token-filtering baseline that scores tokens by task relevance, novelty, or reasoning-related criteria.
- **ssTOKEN (Qin et al., 2026):** A selective response-token training baseline under a fixed retained-token budget.

- **Wise-FT** (Wortsman et al., 2022): A forgetting-resistant baseline that interpolates pre-trained and fine-tuned weights.
- **FLOW** (Sanyal et al., 2025): A conservative fine-tuning baseline that upweights easier or more stable samples to reduce forgetting.
- **TALR** (Lin et al., 2026): A token-level reweighting baseline that suppresses unstable token updates during fine-tuning.

Preference-alignment baselines. For preference optimization, all methods start from the same UltraChat-200k SFT warm-start checkpoint and train on the same UltraFeedback preference data.

- **Base:** The UltraChat-200k warm-started model before preference optimization.
- **DPO** (Rafailov et al., 2023): The standard sequence-level preference-optimization baseline.
- **ConfPO** (Yoon et al., 2025): A confidence-aware preference-optimization baseline that downweights uncertain preference signals.
- **SePO** (Yang et al., 2025): A selective preference-optimization baseline that applies preference gradients to more informative response parts.
- **TI-DPO** (Yang et al., 2026a): A token-importance-based DPO baseline that reweights or selects influential tokens in preference pairs.

AlphaToken differs from these baselines by estimating response-token value through gradient alignment, decomposing it into adaptation and stability terms, and further separating direct and causal-path effects.

C.2 Training Data Details

We use separate training data for supervised fine-tuning and preference optimization. For supervised fine-tuning, we use Magicoder (Wei et al., 2024) as the target-task corpus. Magicoder is an instruction-code dataset designed for code generation, where each instance contains a natural-language programming instruction and a reference solution. We train SFT models by applying the standard causal language-modeling objective only on response tokens, with AlphaToken or the corresponding baseline deciding which response-token losses are retained when token selection is used.

For preference optimization, we follow a two-stage training pipeline. First, each pre-trained backbone is warm-started with supervised fine-tuning

Table 4: Summary of training datasets used in our experiments.

Dataset	Usage	Size
Magicoder	SFT target-task training for code generation	75K instructions
UltraChat-200k	SFT warm-start for preference optimization	200K conversations
UltraFeedback	Preference optimization	63.6K preference pairs

on UltraChat-200k (Ding et al., 2023), which provides multi-turn instruction-following conversations and converts the base model into a chat-capable reference model. Second, preference optimization is performed on UltraFeedback (Bartolome et al., 2023). We use the binarized preference format, where each instance pairs a prompt with a preferred response and a rejected response, enabling DPO-style objectives to increase the relative likelihood of the preferred response over the rejected one. All preference-alignment baselines and AlphaToken use the same warm-start checkpoint and preference-training split. Table 4 summarizes the training datasets used in our experiments.

C.3 Evaluation Details

We evaluate model performance from two perspectives: general capability retention and post-training target performance. For supervised fine-tuning, HumanEval (Chen et al., 2021) is used as the target-task benchmark for code generation, while ARC-C (Clark et al., 2018), HellaSwag (Zellers et al., 2019), MMLU (Hendrycks et al., 2021), and GSM8K (Cobbe et al., 2021) evaluate general capability retention. For preference optimization, AlpacaEval 2 (Li et al., 2023) and ArenaHard v0.1 (Li et al., 2024) are used to evaluate instruction-following preference performance, while the same four general benchmarks, ARC-C (Clark et al., 2018), HellaSwag (Zellers et al., 2019), MMLU (Hendrycks et al., 2021), and GSM8K (Cobbe et al., 2021), are used to measure retention. All reported numbers are percentages. General Capability Avg. is the arithmetic mean over ARC-C, HellaSwag, MMLU, and GSM8K. For SFT, Overall is the arithmetic mean of General Capability Avg. and HumanEval PASS@1. For preference optimization, Preference Avg. is the arithmetic mean of AlpacaEval 2 and ArenaHard v0.1, and Overall is the arithmetic mean of General Capability Avg. and Preference Avg. Table 5 summarizes the evaluation benchmarks and metrics.

- **ARC-C** (Clark et al., 2018): ARC-Challenge is a multiple-choice science QA benchmark for

Table 5: Evaluation benchmarks and detailed settings.

Benchmark	Aspect	Metric	Setting
ARC-C	General capability retention	Accuracy	0-shot
HellaSwag	General capability retention	Accuracy	0-shot
MMLU	General capability retention	Accuracy	5-shot
GSM8K	General capability retention	Exact-match accuracy	5-shot
HumanEval	SFT target-task adaptation	PASS@1	0-shot
AlpacaEval 2	Preference optimization	Win rate	Standard judge
Arena-Hard v0.1	Preference optimization	Win rate	Standard judge

grade-school scientific reasoning. Each question requires selecting the correct answer from several candidates. We report Accuracy.

- **HellaSwag** (Zellers et al., 2019): HellaSwag evaluates commonsense natural language inference. Given an event description or partial context, the model selects the most plausible continuation from candidates. We report Accuracy.
- **MMLU** (Hendrycks et al., 2021): Massive Multitask Language Understanding evaluates knowledge and reasoning across domains, including STEM, humanities, social sciences, and professional knowledge. We report 5-shot Accuracy.
- **GSM8K** (Cobbe et al., 2021): GSM8K evaluates mathematical reasoning on grade-school word problems. The model must generate a numerical answer after multi-step reasoning. We report exact-match accuracy after answer extraction.
- **HumanEval** (Chen et al., 2021): HumanEval evaluates correctness for code generation. Each problem provides a Python function signature and natural-language description, and the solution is judged by hidden unit tests. We report PASS@1 with one solution per problem.
- **AlpacaEval 2** (Li et al., 2023): AlpacaEval 2 evaluates instruction-following through pairwise automatic judging. The judge compares model responses against reference or baseline responses under the official protocol. We report win rate.
- **Arena-Hard v0.1** (Li et al., 2024): Arena-Hard v0.1 is a challenging instruction-following benchmark designed to better separate strong aligned models. It uses pairwise automatic judging on hard user queries. We report win rate.

We use the following metrics in our experiments.

- **Accuracy (ACC)** measures the proportion of correct predictions across examples. For multiple-choice benchmarks, the prediction is correct if

the selected option matches the reference answer:

$$\text{ACC} = \frac{1}{N} \sum_{i=1}^N \mathbb{1}[\hat{y}_i \in \mathcal{Y}_i], \quad (44)$$

where N is the number of evaluation examples, \hat{y}_i is the model prediction, and \mathcal{Y}_i is the set of acceptable answers for the i -th example.

- **Exact Match (EM)** measures whether the normalized prediction exactly matches the normalized reference answer:

$$\text{EM} = \frac{1}{N} \sum_{i=1}^N \mathbb{1}[\text{norm}(\hat{y}_i) = \text{norm}(y_i)], \quad (45)$$

where y_i is the reference answer and $\text{norm}(\cdot)$ denotes the benchmark-specific answer normalization function.

- **PASS@1** measures whether a single generated program passes all unit tests for a HumanEval problem:

$$\text{PASS@1} = \frac{1}{N} \sum_{i=1}^N \mathbb{1}[\text{tests}(\hat{c}_i) = 1], \quad (46)$$

where \hat{c}_i is the generated code for the i -th problem and $\text{tests}(\hat{c}_i) = 1$ indicates that all associated unit tests are passed.

- **Win Rate (WR)** measures the pairwise preference performance on AlpacaEval 2 and Arena-Hard v0.1:

$$\text{WR} = \frac{N_{\text{win}} + 0.5 N_{\text{tie}}}{N}, \quad (47)$$

where N_{win} and N_{tie} denote the number of wins and ties assigned by the automatic judge, and N is the total number of judged examples.

C.4 Implementation Details

All methods are implemented under a unified post-training setup and optimized with AdamW using a cosine learning-rate scheduler. We use bfloat16 mixed-precision training and gradient checkpointing for all backbones. For supervised fine-tuning on Magicoder (Wei et al., 2024), we use a global batch size of 64, a maximum sequence length of 4096, and train for 3 epochs. For preference optimization, we first warm-start each pre-trained backbone on UltraChat-200k (Ding et al., 2023) with a global batch size of 128, a maximum sequence length of

2048, and 2 epochs of SFT. We then perform preference optimization on UltraFeedback (Bartolome et al., 2023) with a global batch size of 64 preference pairs, maximum prompt length 1024, maximum response length 1024, and 3 training epochs. The peak learning rate is 2×10^{-5} for Llama-3.2-3B and Gemma-3-4B, and 1×10^{-5} for Qwen-3.5-9B.

For preference optimization training, the SFT warm-start checkpoint is used as the reference model. We set the DPO temperature coefficient to $\beta = 0.1$. The peak learning rate is 2×10^{-6} for Llama-3.2-3B and Gemma-3-4B, and 1×10^{-6} for Qwen-3.5-9B. Hyperparameters are selected according to the target validation split and used for the final run. The same tokenizer, chat template, optimizer, scheduler, batch construction, and evaluation protocol are used for all methods under the same backbone. Package versions, preprocessing scripts, decoding parameters, judge settings, and answer-extraction rules are provided in the anonymous code repository.

For LoRA (Hu et al., 2022), we insert low-rank adapters into the attention and MLP projection layers and tune only the adapter parameters. For data-selection and token-selection baselines, including LESS (Xia et al., 2024), Token Cleaning (Pang et al., 2025), STM (Wu et al., 2025), XTF (Yang et al., 2026b), ssTOKEN (Qin et al., 2026), ConfPO (Yoon et al., 2025), SePO (Yang et al., 2025), and TI-DPO (Yang et al., 2026a), we follow the official implementation and recommended settings. When a method requires a retained-token ratio, we use the same retained ratio as AlphaToken to ensure a matched effective token budget. All experiments are conducted on $4 \times$ NVIDIA A100 GPUs.

C.5 Training and Validation Setup

AlphaToken requires two auxiliary signals during training: a target-side validation gradient and a data-free retention proxy. For the target-side signal, we hold out a validation subset of size $B_{\text{val}} = 32$ from the training corpus. For SFT, this subset is sampled from Magicoder (Wei et al., 2024); for preference optimization, it is sampled from UltraFeedback (Bartolome et al., 2023). These validation examples are used only to compute the target-side gradient signal in Eq. (8) and Eq. (9); they are excluded from parameter optimization.

During AlphaToken training, we concatenate the fixed target-validation mini-batch with each training mini-batch and obtain the validation-side acti-

vation and error signals in the same forward/backward pass. The validation-side token signals are averaged over validation tokens to keep the scale independent of B_{val} . By default, AlphaToken scores response tokens using the last $K = 3$ Transformer layers, causal window $W = 32$, retained-token ratio $\rho = 0.5$, and stability weight $\lambda = 1.5$. The threshold τ_ρ is computed within each training batch, so that each batch retains the top- ρ response tokens according to the composite value in Eq. (12).

For the retention proxy, we construct the diagonal Monte-Carlo Fisher once before training from 1,000 prompts sampled from the current training distribution. For SFT, the reference checkpoint θ_{ref} is the original pre-trained backbone. For preference optimization, θ_{ref} is the UltraChat-200k warm-start checkpoint before DPO optimization. Labels used in the Monte-Carlo Fisher are self-sampled from $p_{\theta_{\text{ref}}}$, so no retention validation data or old-task examples are required. The resulting diagonal Fisher is cached throughout training. At each step, AlphaToken refreshes the layer-wise proxy slice $V^l = F_{W^l} \odot (W^l - W_{\text{ref}}^l)$ and computes the activation-parameter contraction in Eq. (11).

For Alpha-DPO, token values are computed separately for the chosen and rejected responses using the DPO-scaled token-level error signals. The sequence-level DPO coefficient is computed from the unmasked preference logit and detached from the token mask. The chosen and rejected branches use separate within-branch top- ρ thresholds, producing masks m_t^+ and m_t^- . These masks are detached before the final loss computation, so AlphaToken changes only which response-token losses receive gradients and does not introduce second-order gradients through the valuation procedure.

D Extended Experimental Analysis

D.1 Analysis of the Fisher-Drift Proxy

AlphaToken replaces the inaccessible retention-validation gradient with a Fisher-drift proxy. Rather than exactly reproducing the oracle retention gradient, the proxy is expected to rank response tokens whose path-aware gradients are compatible with preserving the reference model. For diagnosis, we build a small oracle retention set with 32 held-out examples, including 8 examples from each of ARC-C, HellaSwag, MMLU, and GSM8K. These examples are used only for this analysis and are excluded from training, Fisher construction, hyperparameter tuning, and model selection.

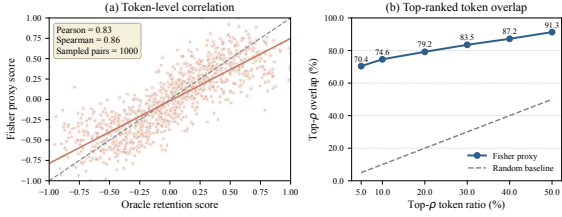


Figure 5: Left: correlation between normalized proxy and oracle retention scores. Right: Top- ρ overlap between proxy- and oracle-selected tokens.

Table 6: Fisher comparison on Llama-3.2-3B/SFT.

Variant	Retention Avg.	HE	Overall	Rel. Time
No Fisher proxy	43.18	44.36	43.77	0.94 ×
Diagonal Fisher	45.47	43.98	44.73	1.00×
Kronecker Fisher	45.56	44.02	44.79	1.28×

For each response token, we compare its Fisher proxy score with its oracle retention-gradient score computed from the held-out retention set. Since raw gradient inner products are scale-dependent and heavy-tailed, both scores are linearly normalized to $[-1, 1]$ for visualization only, preserving the token ranking used in the Top- ρ analysis.

As shown in Fig. 5, the Fisher proxy is strongly correlated with oracle retention-gradient scores and achieves much higher Top- ρ overlap than random selection, supporting its use as a reliable ranking signal for retention-aware token selection.

We further study whether the diagonal Fisher approximation used in AlphaToken is sufficient for the data-free retention proxy on Llama-3.2-3B/SFT. Table 6 compares the default diagonal Fisher with a more expensive Kronecker-factored approximation, which preserves layerwise input-output correlations in the scoring layers. All other settings, including the retained-token ratio, causal window, scoring layers, validation batch, and training protocol, are kept fixed.

The Kronecker Fisher brings only a small improvement over the diagonal approximation while substantially increasing scoring cost. In contrast, diagonal Fisher achieves nearly the same retention and overall performance with much lower overhead. Removing the Fisher proxy yields slightly higher target adaptation but noticeably weaker retention, confirming the importance of the Fisher-weighted drift signal. These results support diagonal Fisher as a practical default for AlphaToken.

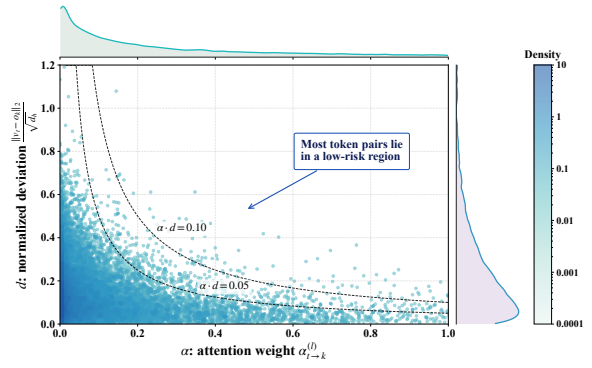


Figure 6: Value-Propagation approximation diagnostics. We visualize the joint distribution of attention weight $\alpha_{t \rightarrow k}^l$ and normalized value-output deviation $d = \|\mathbf{v}_t - \mathbf{o}_k\|_2 / \sqrt{d_h}$ over causal-window token pairs. Marginal density curves are shown on the top and right. Dashed curves indicate constant approximation-risk levels measured by $\alpha \cdot d$. Most token pairs concentrate in low-risk regions, suggesting that the omitted score-propagation term is typically limited.

D.2 Value-Propagation Approximation Diagnostics

Figure 6 provides an empirical diagnostic for the Value-Propagation approximation used in the causal path. We collect causal-window token pairs from the scoring layers during training and visualize the joint distribution of the attention weight $\alpha_{t \rightarrow k}^l$ and the normalized value-output deviation $d = \|\mathbf{v}_t - \mathbf{o}_k\|_2 / \sqrt{d_h}$. The top and right marginal curves show that both quantities are highly skewed toward small values. More importantly, most token pairs concentrate in the lower-left region of the joint space, indicating that they either receive small attention weights, have small value-output deviation, or both.

The dashed curves mark levels of the product $\alpha \cdot d$, which serves as a proxy for the approximation-risk factor appearing in the Value-Propagation error bound. The distribution shows that high-risk pairs with large attention weight and large value-output deviation are rare, while most token pairs fall below the low-risk contours. This pattern supports Value-Propagation as a practical causal-path estimator: for most token pairs encountered during training, the residual score-dependent component remains concentrated in low-risk regions.

D.3 Token-Coverage Effect of AlphaToken

We further examine whether the causal-path term changes the types of response tokens selected by AlphaToken. We visualize contextual embeddings under four policies: random selection, low-

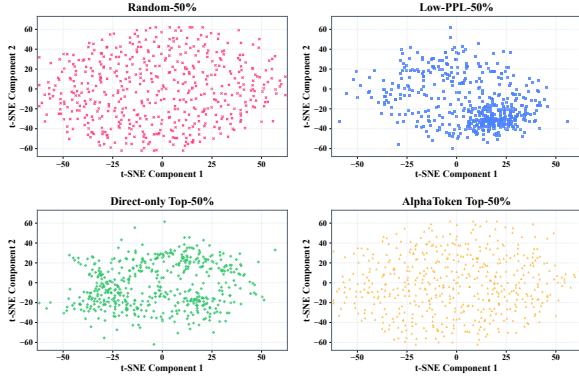


Figure 7: t-SNE visualization of contextual embeddings of selected response tokens. All policies retain 50% of response tokens and use the same t-SNE space fitted on all selected token embeddings. Low-PPL selection concentrates in a narrower region, while Direct-only favors locally salient tokens. AlphaToken covers the space more evenly, suggesting that the causal-path term selects tokens with more diverse contextual roles.

perplexity selection, direct-only valuation, and full AlphaToken, all retaining 50% of tokens. For comparability, we fit one t-SNE projection on the union of selected embeddings and use the same two-dimensional coordinates for all policies.

Figure 7 shows that Low-PPL selection concentrates in a narrow embedding region, suggesting a preference for easy or fluent tokens. Direct-only valuation covers a broader region but remains visibly clustered, indicating that local signals may miss broader downstream-context roles. In contrast, AlphaToken distributes selected tokens more evenly, suggesting that the causal-path term recovers tokens with diverse contextual roles rather than only strong immediate signals. Random selection also covers a broad region, but unlike AlphaToken, it is not value-aware and does not distinguish tokens by their contribution to adaptation or retention.

D.4 Retention-Probe Representation Stability

We examine whether AlphaToken better preserves the representation geometry of general-capability inputs after fine-tuning. We sample 1,000 *HelLaSwag* prompts as retention probes and feed them into the pre-trained and fine-tuned models. For each prompt, we mean-pool the last-layer hidden states over non-padding tokens. For each backbone, we fit a shared t-SNE projection over pre-trained and post-fine-tuning representations, and visualize Standard FT and AlphaToken under the space.

Figure 8 shows that Standard FT causes a clear distributional shift across all three backbones, re-

flected by displaced point clouds, marginal densities, and confidence ellipses. This suggests that direct target optimization substantially perturbs the representation geometry of retention probes. In contrast, AlphaToken produces post-fine-tuning representations that overlap more closely with the pre-trained distributions across Llama-3.2-3B, Gemma-3-4B, and Qwen-3.5-9B.

These results complement the main retention metrics. By selectively allocating gradient flow to high-value response tokens, AlphaToken reduces updates from less useful positions and better constrains representation-level drift, supporting its improved adaptation–retention trade-off.

D.5 Qualitative Token-Level Visualizations

To complement Sec. 5.6, we provide additional qualitative visualizations on three SFT training examples. While Sec. 5.6 decomposes AlphaToken into four components on one dynamic-programming example, this appendix visualizes the final token value Φ on more response fragments. Scores are normalized within each example, with darker colors indicating higher relative value.

Figure 9 shows that high-value tokens often align with structurally important program elements. In the AVL-tree example, they concentrate around height updates, balance-factor checks, and rotations such as `leftRotate` and `rightRotate`. In the linked-list example, AlphaToken highlights pointer-manipulation tokens for insertion and reversal, including `newNode.next`, `current.next`, `prev`, `nextNode`, and the final head update. In the GridMaster example, high-value tokens appear around DFS/BFS control flow, including direction maps, inverse moves, target detection, recursive exploration, and backtracking.

These examples suggest that Φ is not uniformly distributed over tokens, but emphasizes tokens governing control flow, state transitions, pointer updates, and search behavior. This provides qualitative evidence that AlphaToken selects semantically and causally meaningful response positions across SFT coding tasks, rather than surface-level or uniformly distributed tokens.

D.6 Running Time Analysis

We evaluate the efficiency of response-token selection methods on Llama-3.2-3B under matched hardware and training settings. We focus on methods with explicit token scoring, selection, masking, or reweighting modules. Train Time denotes the

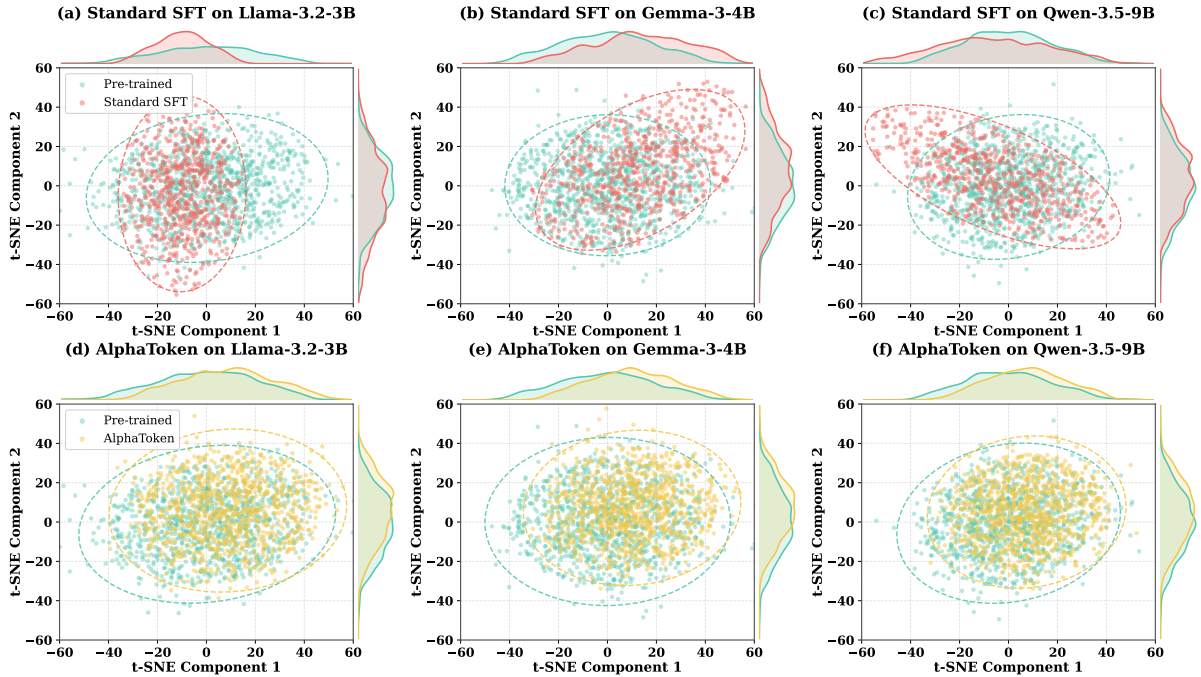


Figure 8: Retention-probe representation stability. We visualize t-SNE distributions of pre-trained and post-fine-tuning prompt representations on 1,000 HellaSwag retention probes. Standard FT induces larger shifts, while AlphaToken keeps post-fine-tuning representations closer to the pre-trained distribution across three backbones.

Table 7: Efficiency profile of token selection methods in SFT on Magicoder with Llama-3.2-3B. Train Time denotes one complete training epoch, and Peak Sel. Mem. denotes peak GPU memory during response-token scoring and mask construction.

Method	Train Time (h/epoch)	Peak Sel. Mem. (GB)
Token Cleaning	5.92	18.74
STM	6.31	21.58
XTF	6.57	24.36
ssTOKEN	6.48	23.91
AlphaToken	7.34	28.62

wall-clock time for one training epoch, including scoring or selection, mask construction, and parameter updates. Peak Sel. Mem. records the maximum GPU memory during response-token scoring and mask construction. SFT is measured on Magicoder, while preference optimization is measured on UltraFeedback after the shared UltraChat-200k warm-up. One-time preprocessing, such as constructing and caching the Monte-Carlo Fisher, is excluded.

Table 7 reports the SFT efficiency profile. Token Cleaning is the cheapest because it mainly uses local discrepancy signals. STM, XTF, and ssTOKEN add token-level scoring or filtering, leading to moderately higher time and memory. AlphaToken further introduces path-aware adapta-

Table 8: Efficiency profile of response-token selection methods in preference optimization on UltraFeedback with Llama-3.2-3B. Train Time denotes one complete training epoch, and Peak Sel. Mem. denotes peak GPU memory during scoring and mask construction over chosen and rejected responses.

Method	Train Time (h/epoch)	Peak Sel. Mem. (GB)
ConfPO	5.58	18.96
SePO	6.24	22.47
TI-DPO	6.43	23.68
AlphaToken	7.72	30.14

tion and stability valuation, with memory mainly from target-side validation signals and activation-parameter contraction for the Fisher-drift proxy. Its runtime remains practical while providing stronger adaptation-retention performance.

Table 8 reports the preference-optimization efficiency profile. ConfPO has the lowest cost because its selection signal relies on policy confidence. SePO and TI-DPO add token-level preference filtering or importance estimation. AlphaToken scores both chosen and rejected responses with target-alignment and stability-proxy signals, introducing extra valuation cost. The overhead remains moderate relative to preference-token selection baselines, and the scoring memory fits within

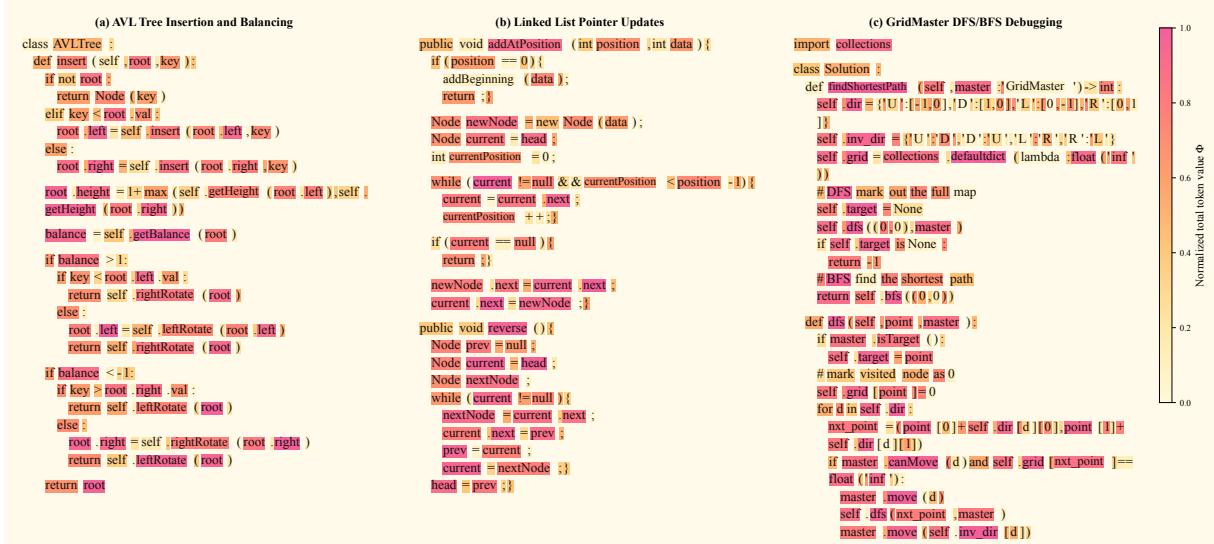


Figure 9: Additional qualitative token-level visualizations on SFT examples. We visualize the final AlphaToken token value Φ on three response fragments from the training data: (a) AVL-tree insertion and balancing, (b) linked-list pointer updates, and (c) GridMaster DFS/BFS debugging. Scores are normalized within each example. Darker colors indicate higher relative token value. AlphaToken assigns higher values to structurally important tokens, including balance checks and rotations, pointer updates, and DFS/BFS control-flow operations.

A100-class GPUs. Overall, AlphaToken achieves a practical runtime and memory profile while improving the adaptation–retention trade-off.

D.7 More Datasets and Baselines

We further evaluate AlphaToken under an additional target domain and stronger forgetting-resistant baselines. Table 9 reports results on MetaMathQA, where GSM8K is the target benchmark and HumanEval is part of general-capability retention. Standard FT achieves the highest GSM8K score but suffers a clear drop in general capability. In contrast, AlphaToken obtains the best Overall score and General Capability Avg., while maintaining the second-best GSM8K performance. This shows that AlphaToken better balances mathematical adaptation and retained general capabilities.

Table 10 compares AlphaToken with forgetting-resistant baselines on Magicoder. Wise-FT and FLOW improve retention over Standard FT, and TALR gives the strongest competing trade-off. AlphaToken still achieves the best Overall score, outperforming TALR by 0.95 points, and also obtains the highest HumanEval and General Capability Avg. These results indicate that path-aware response-token valuation remains effective against dedicated forgetting-mitigation methods.

D.8 Preference-Optimization Ablations

Table 11 ablates AlphaToken under the preference-optimization setting on Gemma-3-4B. We evaluate three groups of design choices. First, we remove either the adaptation or stability objective to test whether the two valuation objectives are complementary. Second, we keep only the direct or causal path to test whether immediate token-level signals and downstream autoregressive influence provide non-redundant information. Third, we ablate two DPO-specific masking designs: using a shared threshold for chosen and rejected responses, and computing the DPO coefficient from the masked preference logit instead of the unmasked sequence-level logit. The ablation results show three trends. First, the objective-axis variants expose the target–retention trade-off in preference optimization. Adaptation-only achieves the highest preference score, improving Preference Avg. from 29.63 to 31.06, but reduces General Capability Avg. from 44.42 to 42.73, indicating a stronger alignment tax when the retention proxy is removed. In contrast, Stability-only obtains the best retention score but substantially weakens preference learning, reducing Preference Avg. to 23.40. Second, the path-axis variants show that direct and causal signals are complementary. Direct-only preserves more of the full model’s performance than Causal-only, but both underperform the full de-

Table 9: MetaMathQA fine-tuning results on Gemma-3-4B. The target task is GSM8K. HumanEval (HE) is reported as part of general capability to assess code-generation retention. Pre-trained models are excluded from color ranking. The best and second-best results are highlighted in red and blue, respectively.

Model	Method	General Capability Acc. (%)					Target (%)	Overall
		ARC-C	HellaSwag	MMLU	HE	Avg.	GSM8K	Avg.
Gemma-3-4B	Pre-trained	51.47 \pm 0.00	57.36 \pm 0.00	59.58 \pm 0.00	35.40 \pm 0.00	50.95 \pm 0.00	36.96 \pm 0.00	43.96 \pm 0.00
	Standard FT	43.52 \pm 0.45	51.40 \pm 0.38	52.96 \pm 0.40	28.90 \pm 0.49	44.20 \pm 0.22	67.65 \pm 0.41	55.93 \pm 0.24
	LoRA ICLR 2022	48.96 \pm 0.36	54.88 \pm 0.28	55.92 \pm 0.32	29.93 \pm 0.51	47.42 \pm 0.19	62.45 \pm 0.37	54.94 \pm 0.21
	LESS ICML 2024	49.97 \pm 0.34	55.94 \pm 0.30	55.34 \pm 0.29	30.42 \pm 0.44	47.92 \pm 0.17	65.42 \pm 0.38	56.67 \pm 0.21
	Token Cleaning ICML 2025	50.15 \pm 0.38	55.31 \pm 0.35	55.72 \pm 0.34	30.58 \pm 0.44	47.94 \pm 0.19	63.20 \pm 0.40	55.57 \pm 0.22
	STM NeurIPS 2025	49.53 \pm 0.40	55.70 \pm 0.34	56.40 \pm 0.27	31.66 \pm 0.51	48.32 \pm 0.19	64.15 \pm 0.39	56.24 \pm 0.22
	XTF ICLR 2026	48.56 \pm 0.39	54.05 \pm 0.35	55.80 \pm 0.33	30.80 \pm 0.52	47.30 \pm 0.20	61.92 \pm 0.37	54.61 \pm 0.22
	ssTOKEN ICLR 2026	49.74 \pm 0.37	54.66 \pm 0.31	56.62 \pm 0.34	31.16 \pm 0.51	48.05 \pm 0.19	63.60 \pm 0.40	55.82 \pm 0.22
	AlphaToken	50.74 \pm 0.30	56.21 \pm 0.29	57.83 \pm 0.28	33.27 \pm 0.34	49.51 \pm 0.15	66.18 \pm 0.39	57.85 \pm 0.19

Table 10: Magicoder fine-tuning results on Gemma-3-4B with forgetting-resistant baselines. Pre-trained models are excluded from color ranking. The best and second-best results are highlighted in red and blue, respectively.

Model	Method	General Capability Acc. (%)					Target (%)	Overall
		ARC-C	HellaSwag	MMLU	GSM8K	Avg.	HE	Avg.
Gemma-3-4B	Pre-trained	51.45 \pm 0.00	56.86 \pm 0.00	59.60 \pm 0.00	37.00 \pm 0.00	51.23 \pm 0.00	35.36 \pm 0.00	43.30 \pm 0.00
	Standard FT	50.17 \pm 0.45	52.63 \pm 0.38	53.87 \pm 0.40	24.12 \pm 0.28	45.20 \pm 0.19	58.79 \pm 0.49	52.00 \pm 0.26
	Wise-FT CVPR 2022	50.32 \pm 0.36	54.46 \pm 0.32	56.03 \pm 0.33	33.40 \pm 0.42	48.55 \pm 0.18	55.92 \pm 0.44	52.24 \pm 0.24
	FLOW ICML 2025	50.83 \pm 0.34	55.72 \pm 0.30	56.46 \pm 0.29	34.28 \pm 0.37	49.32 \pm 0.16	58.34 \pm 0.44	53.83 \pm 0.23
	TALR ICLR 2026	51.02 \pm 0.30	56.06 \pm 0.34	57.88 \pm 0.25	35.61 \pm 0.41	50.14 \pm 0.17	60.37 \pm 0.51	55.26 \pm 0.27
	AlphaToken	51.10 \pm 0.30	55.12 \pm 0.29	58.22 \pm 0.28	36.58 \pm 0.46	50.26 \pm 0.17	62.15 \pm 0.34	56.21 \pm 0.19

Table 11: PO ablations on Gemma-3-4B.

Ablation Axis	Variant	Gen.	AE2	A-Hard	Pref. Avg.	Overall
Full design	Full AlphaToken	44.42	31.86	27.40	29.63	37.03
Objective	Adaptation-only	42.73	33.37	28.74	31.06	36.90
	Stability-only	45.08	25.42	21.37	23.40	34.24
Path	Direct-only	44.19	30.17	25.88	28.03	36.11
	Causal-only	43.81	28.46	24.59	26.53	35.17
DPO masking	Shared τ_p for y^+ / y^-	44.05	30.49	26.08	28.29	36.17
	Masked DPO logit	43.66	29.73	25.92	27.83	35.75

sign, suggesting that immediate token gradients and downstream causal influence capture different aspects of preference-relevant token value. Third, the DPO-specific ablations confirm that branch-aware masking is important. Using a shared threshold for chosen and rejected responses weakens preference learning, while computing the DPO coefficient from the masked logit makes the update less stable. These results support the Alpha-DPO design, where chosen and rejected responses are scored with separate within-branch thresholds and the sequence-level DPO coefficient is computed from the unmasked preference logit and detached before token-level masking.

D.9 Preference Optimization Sensitivity

As shown in Table 12, AlphaToken remains robust under preference optimization across moderate hyperparameter ranges. For the retained token ratio ρ , $\rho = 0.4$ best preserves general capability, while $\rho = 0.3$ underfits AE2 and Arena-Hard. The default $\rho = 0.5$ achieves the best Overall score. Larger ratios reduce both preference and retention

metrics, suggesting that low-value tokens introduce noisy gradients.

The stability weight λ controls the balance between adaptation and retention. Smaller values improve preference scores but reduce retention, whereas larger values preserve general capability at the cost of preference learning. The best Overall score appears at $\lambda = 1.5$, indicating that a moderately strong stability proxy reduces alignment tax without over-constraining optimization.

For the causal window W , performance improves from small windows and becomes stable after $W = 32$. We use $W = 32$ as the default because it provides sufficient future token coverage while avoiding the extra cost of larger windows. For scoring layers, larger last- K generally improves performance, but the gain over last- $K = 3$ is modest, making last- $K = 3$ a practical choice for balancing efficiency and performance. Similarly, increasing B_{val} improves valuation stability and becomes stable after $B_{\text{val}} = 32$. We use $B_{\text{val}} = 32$ as the default to obtain stable target gradient estimates while avoiding the higher cost of larger validation batches.

The DPO coefficient β controls preference update strength. A small β preserves general capability but under-optimizes preference learning, while larger values improve AE2 and Arena-Hard at the cost of retention. The default $\beta = 0.10$ ties for the best rounded Overall score while preserving better general capability than $\beta = 0.20$. Overall, AlphaToken is not overly sensitive to any hyperpa-

parameter, and the default setting balances preference learning, retention, and computational cost.

E Artifact Licenses and Intended Use

We use publicly available artifacts, including model checkpoints, training corpora, evaluation benchmarks, and baseline implementations, through their official release channels and in accordance with their licenses, terms of use, and intended research purposes. Magicoder, UltraChat-200K, and UltraFeedback are used for supervised fine-tuning, warm-start instruction tuning, and preference optimization, respectively, while HumanEval, AlpacaEval 2, Arena-Hard, ARC-C, HellaSwag, MMLU, and GSM8K are used only for evaluation. We do not redistribute original datasets, benchmarks, or model weights. Our released code contains implementation scripts, configurations, and reproduction instructions for research use only, and any derivative outputs are used solely for research analysis rather than deployment outside research contexts.

Table 12: Parameter sensitivity of AlphaToken under preference optimization on Gemma-3-4B.

Value	General Capability Acc. (%)					Preference Win Rate (%)			Overall
	ARC-C	HellaSwag	MMLU	GSM8K	Avg.	AE2	A-Hard	Avg.	Avg.
Retained-token ratio ρ									
0.3	50.61	51.53	52.45	24.45	44.76	20.31	16.90	18.61	31.68
0.4	50.92	51.92	52.10	24.34	44.82	27.83	24.00	25.92	35.37
0.5	50.48	51.46	51.68	24.06	44.42	31.86	27.40	29.63	37.03
0.6	49.92	50.94	51.25	23.41	43.88	31.99	26.80	29.40	36.64
0.7	49.57	50.72	51.41	22.92	43.66	29.94	24.40	27.17	35.41
Stability weight λ									
0.6	48.54	49.95	50.26	22.33	42.77	33.29	28.80	31.05	36.91
0.9	49.61	50.68	50.95	23.80	43.76	32.11	27.90	30.01	36.88
1.2	50.86	51.82	52.04	24.24	44.74	30.19	26.00	28.10	36.42
1.5	50.48	51.46	51.68	24.06	44.42	31.86	27.40	29.63	37.03
1.8	51.15	52.16	52.42	24.39	45.03	27.95	23.90	25.93	35.48
Causal window W									
4	50.05	51.04	51.20	23.79	44.02	29.25	25.00	27.13	35.57
8	50.22	51.26	51.43	24.09	44.25	30.87	26.60	28.74	36.49
16	50.46	51.43	51.70	24.01	44.40	31.93	27.50	29.72	37.06
32	50.48	51.46	51.68	24.06	44.42	31.86	27.40	29.63	37.03
64	50.42	51.40	51.69	23.97	44.37	31.99	27.50	29.75	37.06
Last-K scoring layers									
1	49.98	50.92	51.15	23.79	43.96	30.12	25.70	27.91	35.94
2	50.20	51.18	51.42	24.00	44.20	31.06	26.80	28.93	36.57
3	50.48	51.46	51.68	24.06	44.42	31.86	27.40	29.63	37.03
5	50.54	51.50	51.76	24.12	44.48	31.99	27.50	29.75	37.11
8	50.58	51.56	51.82	24.12	44.52	32.05	27.60	29.83	37.17
Target validation size B_{val}									
4	50.02	51.12	51.34	23.72	44.05	30.75	26.50	28.63	36.34
8	50.27	51.30	51.54	23.97	44.27	31.24	27.00	29.12	36.70
16	50.54	51.51	51.74	24.09	44.47	31.93	27.50	29.72	37.09
32	50.48	51.46	51.68	24.06	44.42	31.86	27.40	29.63	37.03
64	50.58	51.54	51.78	24.10	44.50	31.93	27.50	29.72	37.11
DPO coefficient β									
0.05	50.66	51.58	51.90	24.10	44.56	29.94	25.70	27.82	36.19
0.10	50.48	51.46	51.68	24.06	44.42	31.86	27.40	29.63	37.03
0.20	49.98	51.08	51.52	23.26	43.96	32.30	27.90	30.10	37.03
0.30	49.32	50.64	50.96	22.68	43.40	32.55	28.00	30.28	36.84